Electromotive force due to magnetohydrodynamic fluctuations in sheared rotating turbulence

J. Squire[1,2,*] and A. Bhattacharjee[1]

[1]*Max Planck/Princeton Center for Plasma Physics, Department of Astrophysical Sciences and Princeton Plasma Physics Laboratory, Princeton University, Princeton, New Jersey 08543, USA*

[2]*TAPIR, Mailcode 350-17, California Institute of Technology, Pasadena, California 91125, USA*

(Received 6 August 2015; published 2 November 2015)

This article presents a calculation of the mean electromotive force arising from general small-scale magnetohydrodynamical turbulence, within the framework of the second-order correlation approximation. With the goal of improving understanding of the accretion disk dynamo, effects arising through small-scale magnetic fluctuations, velocity gradients, density and turbulence stratification, and rotation, are included. The primary result, which supplements numerical findings, is that an off-diagonal turbulent resistivity due to *magnetic fluctuations* can produce large-scale dynamo action—the magnetic analog of the "shear-current" effect. In addition, consideration of α effects in the stratified regions of disks gives the puzzling result that there is no strong prediction for a sign of α, since the effects due to kinetic and magnetic fluctuations, as well as those due to shear and rotation, are each of opposing signs and tend to cancel each other.

DOI: 10.1103/PhysRevE.92.053101 PACS number(s): 52.30.−q, 97.10.Gz, 91.25.Cw, 52.35.Ra

I. INTRODUCTION

Explaining the amplification of magnetic fields with correlation lengths larger than the underlying fluid motions has proven to be a fascinating and rich problem in astrophysics. From the early days of mean-field dynamo theory it has been well known that the presence of fluid helicity enables such behavior [1,2]. This is the so-called α effect, where the small-scale turbulence creates an electromotive force (EMF),

$$\boldsymbol{\mathcal{E}} = \langle \boldsymbol{u} \times \boldsymbol{b} \rangle,$$

that is proportional to a large-scale magnetic field, $\boldsymbol{\mathcal{E}} = \alpha \boldsymbol{B}$, leading to exponential instability in the kinematic regime. While this simple α effect is now well established and regularly observed in simulations, a variety of complications exist in explaining observations. For one, in some situations—for instance, the inner regions of accretion disks—there is no reason to expect a helical flow and symmetry arguments demonstrate that $\alpha = 0$, yet dynamo action is still observed in numerical experiments [3,4]. Less obviously, nonlinear effects caused by the fast buildup of small-scale fields can "quench" α dynamos before significant mean-field amplitudes are reached [5,6]. Since the effectiveness of this quenching increases with the Reynolds numbers, it remains unclear whether mean-field theory is able to explain the observed field amplitudes in the nearly dissipation-free plasmas prevalent in astrophysical environments. For these reasons, it is interesting to consider other possibilities for mean-field dynamo action, in particular the effects of velocity gradients and strong homogeneous magnetic fluctuations.

In this paper, we present a very general theoretical examination of different mean-field dynamo effects, within the second-order correlation approximation (SOCA). In particular, we include the effects of specified large-scale velocity gradients, rotation, density and turbulence stratification, helicity, and a bath of strong small-scale magnetic fluctuations (treated in the same way as the velocity fluctuations). For our primary inspiration in this work—the accretion disk dynamo—each of these effects can be important in some way, and this will also be the case in a wide variety of other astrophysical scenarios. Of particular note is the presence of homogeneous magnetic fluctuations, which have not been included in most previous theoretical mean-field dynamo investigations (but see Vainshtein and Kichatinov [7] and Pouquet *et al.* [8] for early treatments, as well as Refs. [9–11]). Magnetic fluctuations should be generically present, at a similar level to velocity fluctuations, in magnetohydrodynamic (MHD) turbulence above moderate Reynolds numbers due to small-scale dynamo action. While SOCA itself cannot capture the small-scale dynamo, by assuming the presence of the magnetic fluctuations we can compute expected changes to the EMF, in particular whether a small-scale magnetic field might suppress, or enhance, kinematic dynamo effects.

The most important result presented here is an analytic confirmation of our numerical work related to the "magnetic shear-current effect" [12,13]. Generically, this type of dynamo is nonhelical, driven by the interaction of an off-diagonal turbulent resistivity with a mean shear flow [14–17]. The kinematic version of this effect has been somewhat controversial, with disagreement between early work [15,17] and subsequent investigations [18,21] over the sign of the crucial transport coefficient η_{yx}. Here, we show that the magnetic version of this effect is much more robust and of the correct sign—not only is its magnitude substantially larger than the kinematic effect, but a variety of calculation methods agree on this: SOCA, the spectral τ approximation [9], quasilinear theory [12,21], and perturbative shearing wave calculations [22]. With this array of other calculations, we feel that SOCA calculations are important, not because they should be more accurate than other methods, but because they are simple, have a well-understood range of validity, and allow exploration of expressions across a range of parameters (e.g., magnetic Prandtl number). This final consideration is notable since it provides the researcher with some indication of the robustness of a given effect, for instance by noting if the sign of a given transport coefficient is particularly sensitive to slight changes in parameters. Finally, all of our results related to η_{yx} have been confirmed through direct numerical simulations [12,13]. Most important is the measurement of a marked decrease in η_{yx} after saturation of

*jsquire@caltech.edu

the small-scale dynamo in sheared turbulence, accompanied by excitation of a coherent mean-field dynamo [13].

Turbulence and density stratification is invariably significant in astrophysical scenarios, including in accretion disks away from the central plane of the disk. With this application in mind, we also apply our results to the case of stratified rotating turbulence with strong velocity shear, considering the resulting α effects. We find that for a Keplerian (or more generally, anticyclonic) rotation profile, the contributions from shear and rotation, and those from kinetic and magnetic fluctuations, are each of opposite signs. The dominant contribution will depend strongly on the magnetic Prandtl number Pm, as well as the relative intensities of magnetic and kinetic turbulence. This is confusing in light of the beautifully coherent "butterfly diagrams" that are often seen in stratified accretion-disk simulations [23–26], which would suggest a robust negative value for α_{yy}. We note that the contributions to these α effects from velocity shear are at least as strong as those from rotation and should not generally be neglected.

Before continuing, it seems worth discussing how the linear transport coefficients presented in this work might be applied to understanding magnetic field generation observed in nature or numerical simulation. In particular, since we assume throughout this work that the mean magnetic field is a small perturbation to the turbulence, the direct applicability of results to turbulence in astrophysical objects is limited. This is particularly true in the presence of magnetic fluctuations, since the large-scale magnetic field will quickly come into equipartition with the (strong) small-scale field due to the finite domain [12], meaning any linear dynamo growth phase is necessarily of limited duration. Thus, rather than expecting quantitative applicability, the presence of a dynamo instability should be taken as an indication that the turbulence will always be accompanied by large-scale structures, presumably in some nonlinearly saturated or time-dependent state. For example, the "butterfly diagram" field migration pattern observed in stratified shearing box simulations could most simply be explained as the saturated state of an $\alpha\omega$ type dynamo, where the field migration is caused by the imaginary part of the dynamo growth rate [see Eq. (12)]. However, there is no particular reason to expect the saturation of the dynamo to be so simple; because the mean field itself strongly influences the turbulence, a wide variety of nonlinear effects are possible beyond a simple dependence of transport coefficients on the mean field, for instance those related to magnetic helicity transport [27] or generation of cross helicity [28] (see Sec. V for further discussion). Similarly, for the magnetic shear-current effect, the linear theory presented here can in no way hope to explain cyclic behavior observed in disk simulations [4,26]. Given their much greater complexity, we leave exploration of these interesting topics to future work.

The structure of our calculation almost identically follows that of Rädler and Stepanov [19] (hereafter RS06), with the additional effects of magnetic fluctuations, density stratification (within an anelastic approximation) and net helicity. The inclusion of such a variety of physical effects leads to a rather prodigious number of terms, and we have used the VEST package [29] in *Mathematica* to carry out the bulk of the calculations. We start, in Sec. II, by outlining the setup of the calculation, including the most general form of $\boldsymbol{\mathcal{E}}$ allowed by the symmetries of the problem, as well as the relation of the transport coefficients in Cartesian domains with velocity shear to this general form. We also give the perturbation expansion used, which is a generalization of that in RS06 to include magnetic turbulence at lowest order. In Sec. III, we outline the procedure used in the calculation itself, skipping many details for the sake of brevity. Particular focus is placed on the unstratified shear dynamo—especially the magnetic shear-current effect—in Sec. IV, while the stratified α effect is examined in the same geometry in Sec. V. Readers interested primarily in the application of calculated coefficients to disk dynamos may wish to skip directly to these sections. Due to the length of algebraic expressions, the full set of transport coefficients is given in Appendix B.

II. FUNDAMENTALS OF MEAN-FIELD ELECTRODYNAMICS

Our starting point, common to most mean-field dynamo calculations, is the system of compressible MHD equations,

$$\begin{aligned}
&\frac{\partial \rho}{\partial t} + \boldsymbol{\nabla}\cdot(\rho \boldsymbol{U}_T) = 0,\\
&\rho\frac{\partial \boldsymbol{U}_T}{\partial t} + \rho(\boldsymbol{U}_T\cdot\boldsymbol{\nabla})\boldsymbol{U}_T + 2\rho\boldsymbol{\Omega}\times\boldsymbol{U}_T + \boldsymbol{\nabla} p\\
&\quad = \boldsymbol{B}_T\cdot\boldsymbol{\nabla}\boldsymbol{B}_T + \boldsymbol{\nabla}\cdot[\rho\nu(\boldsymbol{\nabla}\boldsymbol{U}_T + (\boldsymbol{\nabla}\boldsymbol{U}_T)^T)\\
&\qquad + \rho\bar{\zeta}\delta_{ij}\boldsymbol{\nabla}\cdot\boldsymbol{U}_T] + \boldsymbol{\sigma_u},\\
&\frac{\partial \boldsymbol{B}_T}{\partial t} = \boldsymbol{\nabla}\times(\boldsymbol{U}_T\times\boldsymbol{B}_T) + \eta\nabla^2\boldsymbol{B}_t + \boldsymbol{\sigma_b},\\
&\boldsymbol{\nabla}\cdot\boldsymbol{U}_T = 0, \quad \boldsymbol{\nabla}\cdot\boldsymbol{B}_T = 0.
\end{aligned} \tag{1}$$

Here $\boldsymbol{U}_T$ and $\boldsymbol{B}_T$ are the full velocity and magnetic fields, $\bar{\nu}$ is the kinematic viscosity, $\bar{\zeta}$ is the bulk viscosity (this will not contribute), and $\bar{\eta}$ is the resistivity. We have included the effects of rotation through a mean Coriolis force $(2\rho\boldsymbol{\Omega}\times\boldsymbol{U}_T)$ in the momentum equation. Before calculating transport coefficients from Eq. (1), we shall apply an anelastic approximation [30,31], assuming nearly incompressible fluctuations with $\boldsymbol{\nabla}\cdot(\rho\boldsymbol{u}) = 0$ [see Eq. (2)]. This allows low-order effects due to a mean density gradient to be retained, while still preserving most of the simplicity of an incompressible calculation.

Mean-field dynamo theory [1,2] involves splitting fields into a mean and fluctuating part:

$$\boldsymbol{U}_T = \boldsymbol{U} + \boldsymbol{u}, \quad \boldsymbol{B}_T = \boldsymbol{B} + \boldsymbol{b}, \tag{2}$$

with $\boldsymbol{U} = \langle \boldsymbol{U}_T\rangle$, $\boldsymbol{B} = \langle \boldsymbol{B}_T\rangle$. The averaging operation $\langle\cdot\rangle$ should filter out small scales and satisfy the Reynolds averaging rules (later in the article we will specify $\langle\cdot\rangle$ as a horizontal spatial average). Applying $\langle\cdot\rangle$ to the induction equation leads to the well-known mean-field induction equation

$$\partial_t \boldsymbol{B} = \boldsymbol{\nabla}\times(\boldsymbol{U}\times\boldsymbol{B}) + \boldsymbol{\nabla}\times\boldsymbol{\mathcal{E}} + \nu\triangle\boldsymbol{B}, \tag{3}$$

where $\boldsymbol{\mathcal{E}} = \langle \boldsymbol{u}\times\boldsymbol{b}\rangle$ is the electromotive force (EMF). The goal of mean-field theory is to calculate $\boldsymbol{\mathcal{E}}$ as a function of $\boldsymbol{B}$ and other parameters in the problem (i.e., $\boldsymbol{U}$, Ω, $\boldsymbol{\nabla}\ln\rho$ and the small-scale turbulence statistics), thereby closing Eq. (3). If $\boldsymbol{\mathcal{E}}(\boldsymbol{B})$ is such that a small magnetic field will be reinforced by the small-scale turbulence, a dynamo instability results.

Before commencing with a full calculation of $\boldsymbol{\mathcal{E}}$, it is worth examining the symmetries of the problem. Assuming scale separation between the mean and fluctuating fields, we can Taylor expand the EMF as

$$\mathcal{E}_i = a_{ij} B_j + b_{ijk} B_{j,k} + \cdots \tag{4}$$

where we use the Einstein summation convention and the comma denotes a derivative. The tensors a_{ij} and b_{ijk} are the transport coefficients determined by the turbulence. In keeping with the separation of scales assumption, we shall consider linear $\boldsymbol{B}$ fields $(\boldsymbol{B})_i = B_i + B_{ij} x_j$, velocity fields $(\boldsymbol{U})_i = U_{ij} x_j$, and density $\rho = \rho_0 + \rho_0 \boldsymbol{x} \cdot \boldsymbol{\nabla} \ln \rho$ (the constant velocity part can be removed by Galilean transformation). As in RS06, to cleanly separate different dynamo effects into scalar coefficients, it is helpful to split $\boldsymbol{\nabla U}$ and $\boldsymbol{\nabla B}$ into symmetric and antisymmetric parts,

$$\begin{aligned} U_{ij} &= D_{ij} - A^U_{ij} = D_{ij} - \tfrac{1}{2}\varepsilon_{ijk} W_k, \\ B_{ij} &= (\boldsymbol{\nabla B})^{(s)}_{ij} - A^B_{ij} = (\boldsymbol{\nabla B})^{(s)}_{ij} - \tfrac{1}{2}\varepsilon_{ijk} J_k, \end{aligned} \tag{5}$$

where D_{ij} and $(\boldsymbol{\nabla B})^{(s)}_{ij}$ are the symmetric parts of U_{ij} and B_{ij} respectively (similarly A^U_{ij} and A^B_{ij} are the antisymmetric parts), $\boldsymbol{W} = \boldsymbol{\nabla} \times \boldsymbol{U}$ is the background vorticity, and $\boldsymbol{J} = \boldsymbol{\nabla} \times \boldsymbol{B}$ is the mean current. Due to the assumption $\boldsymbol{\nabla} \cdot \boldsymbol{U} = 0$ in our calculation, we have implicitly assumed $\boldsymbol{U} \cdot \boldsymbol{\nabla} \rho = 0$, a requirement that could easily be relaxed if desired.

We consider general inhomogeneous background turbulence in both $\boldsymbol{u}$ and $\boldsymbol{b}$, modified by mean velocity gradients, rotation, and density stratification. The density stratification is assumed to be aligned with the turbulence stratification in the direction $\hat{\boldsymbol{g}}$, but we allow their magnitudes and signs to differ; that is, defining

$$\boldsymbol{\nabla} \ln \rho = \chi_\rho \hat{\boldsymbol{g}}, \quad \boldsymbol{\nabla} \ln \bar{u} = \chi_{\bar{u}} \hat{\boldsymbol{g}}, \quad \boldsymbol{\nabla} \ln \bar{b} = \chi_{\bar{b}} \hat{\boldsymbol{g}} \tag{6}$$

(where $\bar{u} = \langle u_0^2 \rangle^{1/2}$, $\bar{b} = \langle b_0^2 \rangle^{1/2}$), we allow $\chi_\rho \neq \chi_{\bar{u}} \neq \chi_{\bar{b}}$. For completeness, we include both nonhelical and helical contributions to the turbulence[1] but neglect the effects of inhomogeneity on the helical part.[2] We assume that the EMF due to the background turbulence vanishes, $\langle \boldsymbol{u} \times \boldsymbol{b} \rangle_0 = 0$ (note that, due to the statistical average, this does not necessarily restrict the turbulent cross helicity $\langle \boldsymbol{u} \cdot \boldsymbol{b} \rangle_0$). Such a $\boldsymbol{B}$ independent contribution could be important in some situations (see, for example, Yoshizawa and Yokoi [32]) and the method applied here can be used to calculate well-known effects of this type if desired, for instance the cross-helicity effect [28]. In addition, we do not calculate the components of the Reynolds stress, which would force a mean-field velocity $\boldsymbol{U}$. This is not justified for any particular reason other than our primary interest in the magnetic field dynamics. While it is possible that there are important interactions between $\boldsymbol{U}$ and $\boldsymbol{B}$ that lead to other instabilities [33], we leave their systematic study to future work.

A careful consideration of the symmetry properties of the system leads to the general representation of $\boldsymbol{\mathcal{E}}$ in terms of a set of scalar transport transport coefficients (see RS06 for a full explanation)

$$\begin{aligned} \boldsymbol{\mathcal{E}} = &- \alpha^{(0)}_H \boldsymbol{B} - \alpha^{(D)}_H D_{ij} B_j - \gamma^{(\Omega)}_H \boldsymbol{\Omega} \times \boldsymbol{B} - \gamma^{(W)}_H \boldsymbol{W} \times \boldsymbol{B} \\ &- \alpha^{(\Omega)}_1 (\hat{\boldsymbol{g}} \cdot \boldsymbol{\Omega}) \boldsymbol{B} - \alpha^{(\Omega)}_2 [(\hat{\boldsymbol{g}} \cdot \boldsymbol{B}) \boldsymbol{\Omega} + (\boldsymbol{B} \cdot \boldsymbol{\Omega}) \hat{\boldsymbol{g}}] \\ &- \alpha^{(W)}_1 (\hat{\boldsymbol{g}} \cdot \boldsymbol{W}) \boldsymbol{B} - \alpha^{(W)}_2 [(\hat{\boldsymbol{g}} \cdot \boldsymbol{B}) \boldsymbol{W} + (\boldsymbol{B} \cdot \boldsymbol{W}) \hat{\boldsymbol{g}}] \\ &- \alpha^{(D)} (\varepsilon_{ilm} D_{lj} \hat{g}_m + \varepsilon_{jlm} D_{li} \hat{g}_m) B_j \\ &- (\gamma^{(0)} + \gamma^{(\Omega)} \hat{\boldsymbol{g}} \times \boldsymbol{\Omega} + \gamma^{(W)} \hat{\boldsymbol{g}} \times \boldsymbol{W} + \gamma^{(D)} D_{ij} \hat{g}_j) \times \boldsymbol{B} \\ &- \beta^{(0)} \boldsymbol{J} - \beta^{(D)} D_{ij} J_j - \left(\delta^{(W)} \boldsymbol{W} + \delta^{(\Omega)} \boldsymbol{\Omega}\right) \times \boldsymbol{J} \\ &- \left(\kappa^{(W)} \boldsymbol{W} + \kappa^{(\Omega)} \boldsymbol{\Omega}\right)_j (\boldsymbol{\nabla B})^{(s)}_{ji} - 2\kappa^{(D)} \varepsilon_{ijk} D_{kr} (\boldsymbol{\nabla B})^{(s)}_{jr}. \end{aligned} \tag{7}$$

Here we have conformed to the sign conventions in RS06 and use the Einstein summation convention. The subscript $\cdot_H$ denotes a coefficient that is only allowed by the helical part of the turbulence, while all other coefficients arise only through the nonhelical part. In addition, since we assume small-scale fluctuations in both $\boldsymbol{u}$ and $\boldsymbol{b}$, we further split each transport coefficient into these contributions; e.g., $\kappa^{(W)} = (\kappa^{(W)})_u + (\kappa^{(W)})_b$. Since we work with SOCA in the linear regime (where $\boldsymbol{B}$ is small), these are always additive and can be calculated separately from the $\boldsymbol{u}$ and $\boldsymbol{b}$ turbulent contributions.

A. Cartesian domains

In Sec. IV we shall give specific results for the numerically convenient Cartesian shear dynamo with nonhelical, unstratified background turbulence. This is essentially a generalization of the unstratified shearing box that is often used in accretion-disk simulations. In this case, mean fields depend only on z, $\boldsymbol{U} = -Sx\hat{\boldsymbol{y}}$ (giving $\boldsymbol{W} = -S\hat{\boldsymbol{z}}$), $\boldsymbol{\Omega} = \Omega\hat{\boldsymbol{z}}$, and the mean-field average is defined as an average over x and y, $\langle \cdot \rangle = (L_x L_y)^{-1} \int \cdot \, dx dy$. The mean-field equations simplify to

$$\begin{aligned} \partial_t B_x &= -\eta_{yx} \partial_z^2 B_y + \eta_{yy} \partial_z^2 B_x, \\ \partial_t B_y &= -S B_x - \eta_{xy} \partial_z^2 B_x + \eta_{xx} \partial_z^2 B_y, \end{aligned} \tag{8}$$

where the η_{ij} are defined to be the relevant components of b_{ijk} that are nonzero for the chosen average and mean field. For $B_i = B_{i0} e^{ikz} e^{\Gamma t}$ a coherent dynamo is possible if

$$\begin{aligned} \Gamma = k\left\{-S\eta_{yx} + k^2\left[\eta_{xy}\eta_{yx} + \tfrac{1}{2}(\eta_{xx} - \eta_{yy})^2\right]\right\}^{1/2} \\ -k^2(\eta_{xx} + \eta_{yy}) \end{aligned} \tag{9}$$

has a real part greater than 0. One can neglect the term multiplying k^2 in the square root in Eq. (9) since S is presumed to be large compared to all transport coefficients. This gives $\eta_{21} S < 0$ as a necessary condition for instability. Computing the relationship between Eqs. (7) and (8) shows

$$\begin{aligned} \eta_{yx} = &-S\left[\delta^{(W)} - \tfrac{1}{2}\left(\kappa^{(W)} - \beta^{(D)} + \kappa^{(D)}\right)\right] \\ &+\Omega\left(\delta^{(\Omega)} - \tfrac{1}{2}\kappa^{(\Omega)}\right), \end{aligned}$$

[1] Our primary reasoning for including the helical part of the correlation here has been to check that standard results, e.g., $\alpha^{(0)} \sim \langle \boldsymbol{u} \cdot \boldsymbol{\nabla} \times \boldsymbol{u} \rangle - \langle \boldsymbol{b} \cdot \boldsymbol{\nabla} \times \boldsymbol{b} \rangle$ [8], are obtained using this method.

[2] Stratification of helical turbulence would presumably provide a host of contributions to the resistivity tensor that would likely be much smaller than contributions from the nonhelical fluctuations, due to being higher order. Given the rather immense size of the calculation without such effects, it seemed prudent to ignore these.

$$\eta_{xy} = S\left[\delta^{(W)} - \tfrac{1}{2}\left(\kappa^{(W)} + \beta^{(D)} - \kappa^{(D)}\right)\right] - \Omega\left(\delta^{(\Omega)} - \tfrac{1}{2}\kappa^{(\Omega)}\right), \tag{10}$$

and $\eta_{xx} = \eta_{yy} = \beta^{(0)}$. Note that Eq. (9) only describes the growth due to a coherent dynamo process and fluctuations in α or η that arise in any finite system can cause a dynamo in and of themselves [12,34,35]. We shall specialize to the Cartesian case in Sec. IV and keep $\boldsymbol{U}$ general for the calculation of the transport coefficients listed in Eq. (7).

In Sec. V we give results specific to the case of stratified sheared rotating turbulence. This is motivated by consideration of the upper (or lower) portions of an accretion disk. Again, mean fields depend only on z, $\boldsymbol{U} = -Sx\hat{\boldsymbol{y}}$, $\boldsymbol{\Omega} = \Omega\hat{\boldsymbol{z}}$, and $\hat{\boldsymbol{g}} = \hat{\boldsymbol{z}}$. We neglect off-diagonal resistivity contributions and use $\eta_{xx} = \eta_{yy} = \beta^{(0)}$. The mean-field equations simplify to

$$\begin{aligned}\partial_t B_x &= -a_{yx}\partial_z B_x - a_{yy}\partial_z B_y + \beta^{(0)}\partial_z^2 B_x,\\ \partial_t B_y &= -SB_x + a_{xy}\partial_z B_x + a_{xx}\partial_z B_y + \beta^{(0)}\partial_z^2 B_y.\end{aligned} \tag{11}$$

With $a_{xy} = -a_{yx}$, considering $B_i = B_{i0}e^{ikz}e^{\Gamma t}$, one obtains the growth rate

$$\Gamma = \left(ikSa_{yy}/2 + k^2 a_{yy}a_{xx}\right)^{1/2} + ika_{xy} - k^2\beta^{(0)}. \tag{12}$$

Again, S is presumed large in comparison to all transport coefficients, so we see that any nonzero a_{yy} can lead to instability at sufficiently long wavelength. Of course, in practice there will be a minimum k possible in the system, particularly since a_{yy} arises from a stratification, so a finite a_{yy} will be necessary to overcome the turbulent resistivity. The coefficients in Eq. (11) are related to those in Eq. (7) through $a_{xy} = -a_{yx} = \gamma^{(0)}$ and

$$\begin{aligned}a_{yy} &= S\left(\alpha_1^{(W)} - \alpha^{(D)}\right) - \Omega\,\alpha_1^{(\Omega)},\\ a_{xx} &= S\left(\alpha_1^{(W)} + \alpha^{(D)}\right) - \Omega\,\alpha_1^{(\Omega)}.\end{aligned} \tag{13}$$

B. Perturbation expansion to describe the fluctuations

For the calculation of $\boldsymbol{\mathcal{E}}$ we use the second-order correlation approximation (SOCA), which involves solving linear equations for the fluctuations by neglecting third-order and higher correlations. As such, this is rigorously valid only at low Reynolds numbers where dissipation dominates over nonlinearities for the fluctuations [SOCA can also be valid in the small Strouhal number limit [Eq. (31)]; see Brandenburg and Subramanian [36] for a more thorough discussion]. In addition, we choose to include the shear, rotation, and density stratification perturbatively [17,19], considering only the linear response of transport coefficients to these effects. An analytic calculation with shear included at zeroth order can be found in [21], and some examples of calculations that include nonlinear contributions from other effects can be found in Refs. [9,10,30,31,37]. In a very general calculation, Pipin [11] nonlinearly includes all effects discussed here (although the approach, the "minimal τ approximation," has a somewhat unknown range of validity). We have also computed the magnetic dynamo transport coefficients with nonperturbative shear and rotation using statistical simulation in the shearing box [12].

Following Rüdiger and Kichatinov [31], Kichatinov and Rüdiger [30], and Rüdiger [37], we start by making an anelastic approximation to the full compressible equations, $\boldsymbol{\nabla}\cdot(\rho\boldsymbol{u}) = 0$. This should be valid for weakly compressible turbulence and allows the inclusion of a weak density stratification into the problem, which is important in a wide variety of mean-field dynamos. We shall assume that the large-scale flow is incompressible, since our primary application is to shear flows. It is then more convenient to work in terms of the small-scale momentum [30,31], $\boldsymbol{m} \equiv \rho\boldsymbol{u}$, since the calculation for $\boldsymbol{m}$ proceeds in a similar manner to the incompressible case.

In retaining both strong homogenous velocity and magnetic fluctuations, denoted $\boldsymbol{u}_0$ (or $\boldsymbol{m}_0$) and $\boldsymbol{b}_0$ respectively, we must treat the momentum and induction equations on the same theoretical footing. We start from Eq. (1) by splitting into mean-field and fluctuation equations, applying the anelastic approximation followed by the change of variables $\boldsymbol{u}_0 = \boldsymbol{m}_0/\rho$. We then linearize the small-scale equations and expand $\boldsymbol{m} = \boldsymbol{m}_0 + \boldsymbol{m}^{(0)} + \boldsymbol{m}^{(1)}\ldots$, $\boldsymbol{b} = \boldsymbol{b}_0 + \boldsymbol{b}^{(0)} + \boldsymbol{b}^{(1)}\ldots$, to perturbatively find the change to the background turbulence caused by the shear, rotation, and stratification. This leads to the SOCA equations that will be used to calculate all transport coefficients:

$$\begin{aligned}(\partial_t - \nu\triangle)\boldsymbol{m}^{(0)} &= -[\boldsymbol{m}_0\cdot\boldsymbol{\nabla}\boldsymbol{U} + \boldsymbol{U}\cdot\boldsymbol{\nabla}\boldsymbol{m}_0 - (\boldsymbol{g}_\rho\cdot\boldsymbol{U})\boldsymbol{m}_0] - \boldsymbol{\nabla}p^{(0)} - 2\boldsymbol{\Omega}\times\boldsymbol{m}_0 + \left(\boldsymbol{b}_0\cdot\boldsymbol{\nabla}\boldsymbol{B} + \boldsymbol{B}\cdot\boldsymbol{\nabla}\boldsymbol{b}^{(0)}\right) - \nu\boldsymbol{g}_\rho\cdot\boldsymbol{\nabla}\boldsymbol{m}_0\\ (\partial_t - \nu\triangle)\boldsymbol{m}^{(1)} &= -\left[\boldsymbol{m}^{(0)}\cdot\boldsymbol{\nabla}\boldsymbol{U} + \boldsymbol{U}\cdot\boldsymbol{\nabla}\boldsymbol{m}^{(0)} - (\boldsymbol{g}_\rho\cdot\boldsymbol{U})\boldsymbol{m}^{(0)}\right] - \boldsymbol{\nabla}p^{(1)} - 2\boldsymbol{\Omega}\times\boldsymbol{m}^{(0)} + \left(\boldsymbol{b}^{(0)}\cdot\boldsymbol{\nabla}\boldsymbol{B} + \boldsymbol{B}\cdot\boldsymbol{\nabla}\boldsymbol{b}^{(0)}\right) - \nu\boldsymbol{g}_\rho\cdot\boldsymbol{\nabla}\boldsymbol{m}^{(0)}\\ (\partial_t - \eta\triangle)\boldsymbol{b}^{(0)} &= \rho^{-1}\left[(\boldsymbol{g}_\rho\cdot\boldsymbol{m}_0)\boldsymbol{B} - \boldsymbol{m}_0\cdot\boldsymbol{\nabla}\boldsymbol{B} + \boldsymbol{B}\cdot\boldsymbol{\nabla}\boldsymbol{m}_0 - (\boldsymbol{g}_\rho\cdot\boldsymbol{B})\boldsymbol{m}_0\right] + \boldsymbol{b}_0\cdot\boldsymbol{\nabla}\boldsymbol{U} - \boldsymbol{U}\cdot\boldsymbol{\nabla}\boldsymbol{b}_0,\\ (\partial_t - \eta\triangle)\boldsymbol{b}^{(1)} &= \rho^{-1}\left[(\boldsymbol{g}_\rho\cdot\boldsymbol{m}^{(0)})\boldsymbol{B} - \boldsymbol{m}^{(0)}\cdot\boldsymbol{\nabla}\boldsymbol{B} + \boldsymbol{B}\cdot\boldsymbol{\nabla}\boldsymbol{m}^{(0)} - (\boldsymbol{g}_\rho\cdot\boldsymbol{B})\boldsymbol{m}^{(0)}\right] + \boldsymbol{b}^{(0)}\cdot\boldsymbol{\nabla}\boldsymbol{U} - \boldsymbol{U}\cdot\boldsymbol{\nabla}\boldsymbol{b}^{(0)},\end{aligned} \tag{14}$$

along with divergence constraints for each $\boldsymbol{m}^{(0)}$, $\boldsymbol{b}^{(0)}$, $\boldsymbol{m}^{(1)}$, and $\boldsymbol{b}^{(1)}$. Here $\boldsymbol{g}_\rho \equiv \chi_\rho\hat{\boldsymbol{g}}$ and we have neglected second derivatives of $\boldsymbol{U}$ and ρ, as well as products of $\boldsymbol{\nabla}\boldsymbol{B}$ with χ_ρ [these contributions should vanish in the transport coefficients, since Eq. (7) illustrates that there is no contribution to the resistivity due to $\hat{\boldsymbol{g}}$ at linear order]. In addition, we shall neglect any terms that involve quadratic products of $\boldsymbol{U}$, $\boldsymbol{\Omega}$, and χ_ρ [e.g., $(\boldsymbol{g}_\rho\cdot\boldsymbol{U})\boldsymbol{m}_0$], and expand all terms to linear order to take the Fourier transport of Eq. (14) (see Appendix A).

While it may seem surprising that one requires terms two orders higher than $\boldsymbol{m}_0$ and $\boldsymbol{b}_0$, it is straightforward to see that only considering $\boldsymbol{m}^{(0)}$ and $\boldsymbol{b}^{(0)}$ will not lead to contributions to $\boldsymbol{\mathcal{E}}$ that depend on products of $\boldsymbol{B}$ with $\boldsymbol{U}$ or $\boldsymbol{\Omega}$ (these are the interesting terms in the dynamo, describing the effect of rotation or velocity). With this in mind, the EMF is calculated as

$$\mathcal{E}_{ij} = \langle u_i b_j\rangle = \langle\rho^{-1}m_{0i}b_{0j}\rangle + \langle\rho^{-1}m_{0i}b_j^{(0)}\rangle + \langle\rho^{-1}m_{0i}b_j^{(1)}\rangle + \langle\rho^{-1}m_i^{(0)}b_{0j}\rangle + \langle\rho^{-1}m_i^{(1)}b_{0j}\rangle + \langle\rho^{-1}m_i^{(0)}b_j^{(0)}\rangle. \tag{15}$$

Despite the fact that all the terms in Eq. (15) give some contribution, there are also a large number of terms that contain quadratic products of U_{ij}, Ω_i, χ_ρ, or $\boldsymbol{B}$, which are neglected. As is evident, with background turbulence in both $\boldsymbol{u}$ and $\boldsymbol{b}$ there will be contributions to $\boldsymbol{\mathcal{E}}$ from the Maxwell stress $(\boldsymbol{B}\cdot\boldsymbol{\nabla}\boldsymbol{b}+\boldsymbol{b}\cdot\boldsymbol{\nabla}\boldsymbol{B})$ that one would expect to be of a similar magnitude to the standard kinematic dynamo arising from the Lorentz force $[\boldsymbol{\nabla}\times(\boldsymbol{u}\times\boldsymbol{B})]$. This choice of perturbation expansion is the natural generalization of RS06 to the case with $\boldsymbol{b}_0$ fluctuations (although note that $\boldsymbol{u}^{(1)}$ in RS06 has become $\boldsymbol{u}^{(0)}$ in our notation such that $\boldsymbol{u}$ and $\boldsymbol{b}$ are treated on equal footings). Our results for the kinematic dynamo ($\boldsymbol{b}_0=0$) without density stratification agree with RS06 aside from a single numerical coefficient (see Appendix B).

III. OUTLINE OF THE CALCULATION OF $\boldsymbol{\mathcal{E}}$

Our calculation follows the methods and notation in RS06 and a full explanation is given there. Here we give a very brief outline, in particular the choices involved, with final results given in Appendix B. We have carried out the entire calculation in *Mathematica* using the VEST package [29] to handle abstract tensor manipulations using the Einstein summation convention.

The two-point correlation of two fields $\boldsymbol{v}$ and $\boldsymbol{w}$ is defined as

$$\phi_{ij}^{(vw)}(\boldsymbol{x}_1,t_1;\boldsymbol{x}_2,t_2)=\langle v_i(\boldsymbol{x}_1,t_1)w_j(\boldsymbol{x}_2,t_2)\rangle. \tag{16}$$

It is convenient to write such quantities in the variables

$$\begin{aligned}\boldsymbol{R}&=(\boldsymbol{x}_1+\boldsymbol{x}_2)/2,\ \ \boldsymbol{r}=\boldsymbol{x}_1-\boldsymbol{x}_2,\\ T&=(t_1+t_2)/2,\ \ t=t_1-t_2,\end{aligned} \tag{17}$$

giving

$$\begin{aligned}\phi_{ij}^{(vw)}(\boldsymbol{R},T;\boldsymbol{r},t)=\Big\langle v_i\Big(\boldsymbol{R}+\frac{\boldsymbol{r}}{2},T+\frac{t}{2}\Big)\\ \times\ w_j\Big(\boldsymbol{R}-\frac{\boldsymbol{r}}{2},T-\frac{t}{2}\Big)\Big\rangle.\end{aligned} \tag{18}$$

One then Fourier transforms in the small-scale variable $\boldsymbol{r}$ to obtain

$$\phi_{ij}^{(vw)}(\boldsymbol{R},T;\boldsymbol{r},t)=\int d\boldsymbol{k}\,d\omega\,\tilde{\phi}_{ij}^{(vw)}(\boldsymbol{R},T;\boldsymbol{k},\omega)e^{i(\boldsymbol{k}\cdot\boldsymbol{r}-\omega t)}, \tag{19}$$

with

$$\tilde{\phi}_{ij}^{(vw)}(\boldsymbol{R},T;\boldsymbol{k},\omega)=\int d\boldsymbol{K}\,d\Omega\,\big\langle[\hat{v}]_+[\hat{w}]_-\big\rangle e^{i(\boldsymbol{K}\cdot\boldsymbol{R}-\Omega T)}, \tag{20}$$

where $\hat{v}=\hat{v}(\boldsymbol{k},\omega)$ and $\hat{w}=\hat{w}(\boldsymbol{k},\omega)$ denote the Fourier transforms of v and w, and we use the $[\cdot]_\pm$ notation of RS06,

$$[\hat{f}(\boldsymbol{k},\omega)]_\pm=\hat{f}(\pm\boldsymbol{k}+\boldsymbol{K}/2,\pm\omega+\Omega/2). \tag{21}$$

As in RS06 we shall calculate

$$\begin{aligned}&\mathcal{E}_{ij}(\boldsymbol{R},T;0,0)\\ &=\int d\boldsymbol{k}\,d\omega\,\tilde{\boldsymbol{\mathcal{E}}}_{ij}(\boldsymbol{R},T;\boldsymbol{k},\omega)\\ &=\int d\boldsymbol{K}\,d\Omega\,d\boldsymbol{k}\,d\omega\,\langle[\rho^{-1}\hat{m}_i]_+[\hat{b}_i]_-\rangle e^{i\boldsymbol{K}\cdot\boldsymbol{R}-i\Omega T}\\ &=\int d\boldsymbol{K}\,d\Omega\,d\boldsymbol{k}\,d\omega\rho_0^{-1}\\ &\quad\times\big\langle[\hat{m}_i-ig_{\rho j}\partial_{k_j}\hat{m}_i]_+[\hat{b}_i]_-\big\rangle e^{i\boldsymbol{K}\cdot\boldsymbol{R}-i\Omega T},\end{aligned} \tag{22}$$

setting $\boldsymbol{R},T\to 0$ only after extracting the coefficients of B_i and B_{ij} (i.e., the transport coefficients a_{ij}, b_{ijk}).

With these notations defined, the starting point of the calculation is the substitution of the linear forms for $\boldsymbol{U}$, ρ, and $\boldsymbol{B}$ and into Eq. (14), followed by a Fourier transform. This leads to Eqs. (A2)–(A5). One then substitutes $\hat{m}_i^{(0)}$ and $\hat{b}_i^{(0)}$ into $\hat{m}_i^{(1)}$ and $\hat{b}_i^{(1)}$ to form explicit expressions for $\hat{u}_i$ and $\hat{b}_i$ in terms of $\hat{u}_{0i}$ and $\hat{b}_{0i}$. Defining

$$\begin{aligned}\tilde{m}_{ij}&=\langle[\hat{m}_{0i}]_+[\hat{m}_{0j}]_-\rangle,\\ \tilde{b}_{ij}&=\langle[\hat{b}_{0i}]_+[\hat{b}_{0j}]_-\rangle,\end{aligned}$$

to specify the statistics of $\boldsymbol{u}_0$ and $\boldsymbol{b}_0$, this allows one to form Eq. (15) in terms of $\tilde{m}_{ij}$ and $\tilde{b}_{ij}$, neglecting all terms that contain $U_{ij}U_{rs}$, $U_{ij}\Omega_j$, $\Omega_i\Omega_r$, $U_{ij}\chi_\rho$, $\Omega_i\chi_\rho$, $(\boldsymbol{\nabla}\ln\rho)^2$, or any products of B_i and B_{ij}. Recall that we have assumed $\langle\boldsymbol{u}_0\boldsymbol{b}_0\rangle=0$, implying that all terms in the expansion of $\mathcal{E}_{ij}$ contain B_i or B_{ij}. In keeping with the expansion to linear order in background quantities, it is necessary to expand $[f(\boldsymbol{k})]_\pm$ to first order in $\boldsymbol{K}$ in those terms that contain B_i (i.e., α coefficients). These lead to terms involving the gradient of the turbulence intensity. Note that $[f(\boldsymbol{k})]_\pm\to f(\pm\boldsymbol{k})$ for resistive terms (coefficients of B_{ij}). Some useful identities in the above procedure are given in RS06 Eqs. (33)–(35), which are needed to remove $\partial/\partial k_i$ derivatives from u_{0i} and b_{0i}. Similarly, we apply the identities

$$k_i\tilde{m}_{ij}=-\frac{K_i}{2}\tilde{m}_{ij},\quad k_i\tilde{m}_{ji}=\frac{K_i}{2}\tilde{m}_{ji} \tag{23}$$

(and similarly for $\tilde{b}_{ji}$), which arise from the divergence constraints on $\hat{m}_i$ and $\hat{b}_i$.

Extracting the coefficients of B_i and B_{ij} in the expression for $\mathcal{E}_i=\varepsilon_{ijk}\mathcal{E}_{jk}(\boldsymbol{0},0)$, at this stage we have large integral expressions for a_{ij} and b_{ijk} in terms of $\tilde{m}_{ij}$ and $\tilde{b}_{ij}$ and their spatial derivatives [for example, RS06 Eqs. (39)–(40)]. Without further interpretation, such expressions are nearly useless, and it is helpful to insert explicit forms for $\tilde{m}_{ij}$ and $\tilde{b}_{ij}$. Assuming isotropy in the limit of vanishing mean flow and rotation, we insert

$$\begin{aligned}\tilde{m}_{ij}&=\frac{1}{2}\Big[\delta_{ij}-\frac{k_ik_j}{k^2}-\frac{1}{2k^2}(k_iK_j-k_jK_i)\Big]W_m(\boldsymbol{K};k,\omega)\\ &\quad-i\varepsilon_{ijl}\frac{k_l}{k^2}H_u(k,\omega),\\ \tilde{b}_{ij}&=\frac{1}{2}\Big[\delta_{ij}-\frac{k_ik_j}{k^2}-\frac{1}{2k^2}(k_iK_j-k_jK_i)\Big]W_b(\boldsymbol{K};k,\omega)\\ &\quad-i\varepsilon_{ijl}\frac{k_l}{k^2}H_b(k,\omega),\end{aligned} \tag{24}$$

where $k=|k_i|$. Here $W_{m,b}$ represents a nonhelical part and $H_{m,b}$ a helical part of the background turbulence [30,31]. This form for W_m is particularly convenient since it can be shown that to first order in the scale of density variation

$$W_m(\boldsymbol{x};k,\omega)=\rho^2(\boldsymbol{x})W_u(\boldsymbol{x};k,\omega), \tag{25}$$

where $W_u(\boldsymbol{x};k,\omega)$ is a similar function specifying the statistics of $\boldsymbol{u}$ and $W_m(\boldsymbol{x};k,\omega) = \int d\boldsymbol{K} e^{i\boldsymbol{K}\cdot\boldsymbol{x}} W_m(\boldsymbol{K};k,\omega)$ [30]. In this way,

$$\boldsymbol{\nabla} W_m(\boldsymbol{x};k,\omega) = \hat{\boldsymbol{g}}(2\chi_\rho + 2\chi_{\bar{u}}) W_m(\boldsymbol{x};k,\omega), \tag{26}$$

separating the effects due to density and turbulence stratification. Similarly, for the magnetic fluctuations

$$\boldsymbol{\nabla} W_b(\boldsymbol{x};k,\omega) = 2\hat{\boldsymbol{g}}\chi_{\bar{b}} W_b(\boldsymbol{x};k,\omega). \tag{27}$$

It transpires that all terms now depend on $\boldsymbol{k}$ only through k, and all of the integrals can be substantially simplified using

$$\begin{aligned}\int d\boldsymbol{k}\, k_i k_j f(k) &= \frac{1}{3}\delta_{ij}\int dk\, k^2 f(k),\\ \int d\boldsymbol{k}\, k_i k_j k_k k_l f(k) &= \frac{1}{15}\left(\delta_{ij}\delta_{kl} + \delta_{ik}\delta_{jl} + \delta_{il}\delta_{jk}\right)\\ &\quad\times \int dk\, k^4 f(k),\end{aligned} \tag{28}$$

where the integrals over k on the right-hand side of Eq. (28) are taken from $k = 0 \to \infty$. One then splits U_{ij} and B_{ij} using Eq. (5), putting $\mathcal{E}_i$ in the form given by Eq. (7). One can straightforwardly read off the transport coefficients $\alpha_H^{(0)},\ldots,\alpha^{(\Omega)},\ldots,\beta^{(0)},\ldots$, as integrals of the form

$$\begin{aligned}\left(\alpha_H^{(\cdot)}\right)_{u,b} &= 4\pi\int dk\, d\omega\, k^2 \tilde{\alpha}_H^{(\cdot)}(k,\omega) H_{u,b}(k,\omega),\\ \left(\alpha^{(\cdot)}\right)_{u,b} &= 4\pi\int dk\, d\omega\, k^2 \tilde{\alpha}^{(\cdot)}(k,\omega) W_{u,b}(k,\omega),\\ \left(\beta^{(\cdot)}\right)_{u,b} &= 4\pi\int dk\, d\omega\, k^2 \tilde{\beta}^{(\cdot)}(k,\omega) W_{u,b}(k,\omega).\end{aligned} \tag{29}$$

The full list of coefficients $\tilde{\alpha}_H^{(0)},\ldots,\tilde{\alpha}^{(\Omega)},\ldots,\tilde{\beta}^{(0)},\ldots$ is given in Appendix B.

Finally, it is possible to carry out the integrals of the form in Eq. (29) for a specific form of W and H, leading to explicit expressions for the transport coefficients in terms of the physical parameters. A convenient form for examining expressions and plotting is the Gaussian W used in RS06,

$$W_u = u_{\mathrm{rms}}^2 \frac{2\lambda_c^3\tau_c}{3(2\pi)^{5/2}} \frac{(k\lambda_c)^2 e^{-(k\lambda_c)^2/2}}{1+(\omega\tau_c)^2}, \tag{30}$$

with a similar definition of W_b. With this choice, all integrals can be carried out explicitly without further approximation. As in RS06, we shall write such expressions in terms of the nondimensional variables (and ρ_0)

$$\begin{aligned}&\epsilon = b_{\mathrm{rms}}/u_{\mathrm{rms}}, \quad p = \lambda_c^2/\nu\tau_c, \quad q = \lambda_c^2/\eta\tau_c, \quad \mathrm{Pm} = \nu/\eta,\\ &\mathrm{Re} = u_{\mathrm{rms}}\lambda_c/\nu, \quad \mathrm{Rm} = u_{\mathrm{rms}}\lambda_c/\eta, \quad \mathrm{St} = u_{\mathrm{rms}}\tau_c/\lambda_c.\end{aligned} \tag{31}$$

Here Pm, Re, Rm, and St are respectively the magnetic Prandtl number, the fluid Reynolds number, the magnetic Reynolds number, and the Strouhal number. p and q are the ratio of diffusion times, λ_c^2/ν and λ_c^2/η, to the correlation time τ_c. Thus $q \to 0$ denotes the low conductivity limit, while $q \to \infty$ denotes a high conductivity limit (with a similar result for p and fluid diffusivity). A sufficient condition for the validity of SOCA (i.e., neglect of nonlinear terms in the correlation equations) is $\mathrm{Rm} \ll 1$ in the limit $q \to 0$, and $\mathrm{St} \ll 1$ in the limit $q \to \infty$; see Brandenburg and Subramanian [36] and Rädler and Stepanov [19] for more discussion of these validity regimes. In addition, we require that U_{ij} and Ω_i be a small perturbation to the background turbulence. In practice, we shall use these nondimensional variables [Eq. (31)] for plotting transport coefficients.

We have carried out the full sequence of steps detailed above in *Mathematica* using the VEST package [29] to enable straightforward manipulation of tensors in index notation. This has the obvious advantage of handling the very long expressions with ease and making the calculation straightforward to generalize or modify. The sequence of steps is essentially the same as that detailed above. We first define $\boldsymbol{m}^{(0)}$, $\boldsymbol{m}^{(1)}$, $\boldsymbol{b}^{(0)}$, and $\boldsymbol{b}^{(1)}$, insert $\boldsymbol{m}^{(0)}$ and $\boldsymbol{b}^{(0)}$ into $\boldsymbol{m}^{(1)}$ and $\boldsymbol{b}^{(1)}$, then only later remove products that are quadratic in U_{ij}, $\boldsymbol{\Omega}$, or χ_ρ. It is then straightforward to define $[\cdot]_\pm$ operators, their associated product rules, and methods to expand in $\boldsymbol{K}$. This allows the construction of the entirety of $\boldsymbol{\mathcal{E}}$ in one step. Insertion of the explicit forms for $\tilde{m}_{ij}$ and $\tilde{b}_{ij}$ [Eq. (24)] and the partial integration using isotropy [Eq. (28)] is easily carried out using replacement rules. Finally, we decompose products of B_{ij} with U_{ij}, $\boldsymbol{\Omega}$, and $\hat{\boldsymbol{g}}$ into the form given in Eq. (7), allowing the coefficients listed in Appendix (B) to be straightforwardly extracted from the total expression. Finally, if so desired, these can be directly integrated with the specific form of W [Eq. (30)] by carefully substituting the dimensionless variables [Eq. (31)] and using *Mathematica*'s native `Integrate` function. For the interested reader, we include the full calculation notebook in the Supplemental Material [38].

Agreement with previous works

Our results agree with related works of other authors in special limits, including those utilizing different calculation methods. As discussed throughout the work, all results of RS06 are recovered in the limit $\boldsymbol{\nabla}\ln\rho = 0$ [aside from one discrepancy, in $(\beta^{(D)})_u$]. This agrees with Rüdiger and Kitchatinov [18], many results of Pipin [11], including his magnetic contributions (see his Appendix B), as well as the quasilinear methods in Sridhar and Subramanian [39] and Singh and Sridhar [21]. As is well known, there is a discrepancy between these kinematic quasilinear results and those obtained using the τ approximation [9,17], possibly due to a change in sign of η_{yx} with Rm [20]. As seen in Eq. (32) of Pipin [11], his conclusions regarding the kinetic and magnetic contributions to the shear-current effect (with rotation) are are similar to ours. Our results also compare favorably to previous works without velocity gradients, but including magnetic fluctuations. As expected, the helical magnetic α effect has the opposite sign to the kinematic effect, and there is no change to $\beta^{(0)}$ due to the addition of magnetic fluctuations. In addition, the signs of $\delta_u^{(\Omega)}$ and $\delta_b^{(\Omega)}$ agree with the τ approximation calculation of Rädler *et al.* [10] ($\delta_u^{(\Omega)} < 0$, $\delta_b^{(\Omega)} > 0$, although there is not an exact cancellation at $\bar{u} = \bar{b}$ as in Rädler *et al.* [10]).

The α effects arising through stratification and inhomogeneity also show broad agreement with previous works. Because of the linearity of the expansion in $\boldsymbol{\nabla}\ln\rho$, U, and Ω, the density stratification contributes very little to the coefficients, aside from directly through $\boldsymbol{\nabla} W_m$ [Eq. (26)]. This means χ_ρ generally appears together with the turbulent gradient $\chi_{\bar{u}}$.

The one exception to this is the "turbulent diamagnetism" term, $\gamma^{(0)}$, which interestingly depends only on the turbulence gradient, not the density gradient, due to a cancellation (this is in agreement with Kichatinov and Rüdiger [30]). Again our results without mean velocity broadly agree with the τ approximation magnetic turbulence results given in Rädler *et al.* [10], for instance, the fact that $(\gamma^0)_b = -(\gamma^0)_u$ and the opposing signs of the rotational kinematic and magnetic diagonal α effects $(\alpha_1^\Omega)_{u,b}$, with $|(\alpha_1^\Omega)_u| > |(\alpha_1^\Omega)_b|$ (although we see a strong dependence of these parameters on Pm; see Sec. V).

IV. SPECIFIC RESULTS FOR UNSTRATIFIED SHEAR DYNAMOS

In this section we discuss the results pertinent to our primary motivation for this work, the shear dynamo in a Cartesian box. As shown in Eq. (8), in this geometry with a horizontal mean-field average, the number of transport coefficients reduces significantly. We are particularly interested in the sign of the η_{yx} coefficient, which should be most important for dynamo growth due to its coupling with the shear [Eq. (9)]. Here we outline the contribution to η_{yx} from velocity and magnetic fluctuations in the presence of shear, both with and without rotation. This geometry is particularly relevant for the central regions of accretion disks, where there is strong flow shear, stratification may be subdominant, and there is no obvious source of helicity in either velocity or magnetic fluctuations [4].

Utilizing Eq. (10) and the results in listed in Appendix B, one obtains after some impressive cancellations

$$(\eta_{yx})_u^S = \int d\omega\, dk \frac{32\pi k^2 W_u(k,\omega)\,\omega^2\tilde{\eta}^2}{15(\tilde{\eta}^2+\omega^2)^2(\tilde{\nu}^2+\omega^2)}, \tag{32}$$

$$(\eta_{yx})_b^S = \int d\omega\, dk\, 8\pi k^2 \rho^{-1} W_b(k,\omega)\Bigg(\frac{4\omega^4}{15(\tilde{\nu}^2+\omega^2)^3} - \frac{2\tilde{\eta}\tilde{\nu}^3+\tilde{\eta}^2\tilde{\nu}^2+2\omega^2\tilde{\eta}^2+3\omega^4}{15(\tilde{\eta}^2+\omega^2)(\tilde{\nu}^2+\omega^2)^2} + \frac{4\omega^2\tilde{\eta}\tilde{\nu}}{15(\tilde{\eta}^2+\omega^2)^2(\tilde{\nu}^2+\omega^2)}\Bigg), \tag{33}$$

$$(\eta_{yx})_u^\Omega = -\int d\omega\, dk \frac{64\pi k^2 W_u(k,\omega)\omega^2\tilde{\eta}^2}{15(\tilde{\eta}^2+\omega^2)^2(\tilde{\nu}^2+\omega^2)}, \tag{34}$$

$$(\eta_{yx})_b^\Omega = -\int d\omega \times dk \frac{8\pi k^2\rho^{-1}W_b(k,\omega)(\tilde{\nu}^4-12\omega^2\tilde{\nu}^2+3\omega^4)}{15(\tilde{\nu}^2+\omega^2)^3}. \tag{35}$$

Here $\tilde{\nu} = \nu k^2$, $\tilde{\eta} = \eta k^2$, integration over ω is from $-\infty$ to ∞ and over k is from 0 to ∞. We have defined each coefficient such that

$$\eta_{yx} = S\left[(\eta_{yx})_u^S + (\eta_{yx})_b^S\right] + \Omega\left[(\eta_{yx})_u^\Omega + (\eta_{yx})_b^\Omega\right], \tag{36}$$

to keep all signs consistent. Recall from Eq. (9) that with our definition of S, $\eta_{yx}S < 0$ is required for a growing dynamo (note that this is the reverse of RS06). For Keplerian rotation, $\Omega = 2S/3$, since vorticity and rotation are opposite (i.e., anticyclonic) when S and Ω have the same sign.

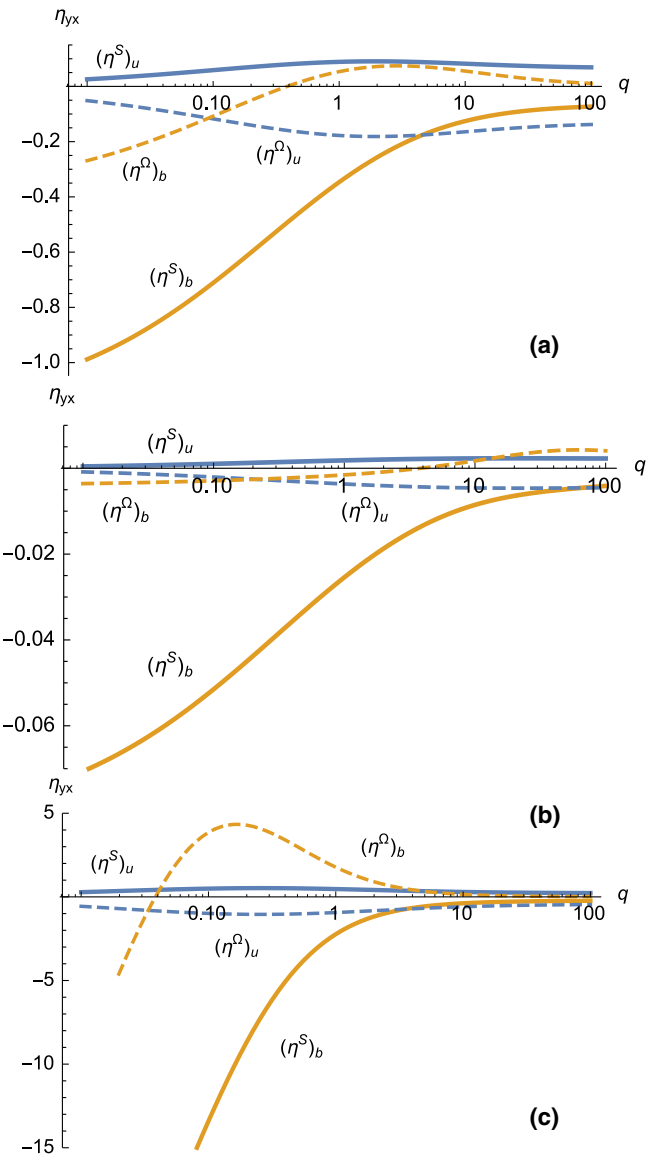

FIG. 1. (Color online) Transport coefficients $(\eta_{yx})_u^S$ (solid, blue), $(\eta_{yx})_u^\Omega$ (dashed, blue), $(\eta_{yx})_b^S$ (solid, orange), and $(\eta_{yx})_b^\Omega$ (dashed, orange) as a function of q for (a) Pm = 1, (b) Pm = 10, and (c) Pm = 1/10 (lines also labeled on each plot). Each coefficient has been calculated using the form given in Eq. (30) for W, and normalized by $(\beta^{(0)})_u$ with the magnetic diffusion time, λ_c^2/η, held constant (equivalently $\tau_c = 1/q$). (Note that this choice is necessary because the coefficients have different units, and is chosen purely for plotting purposes, since it reduces the variation of coefficients with q.)

Let us first examine the coefficients for a kinematic dynamo, i.e., with strong homogeneous velocity fluctuations [the coefficients $(\eta_{yx})_u$, Eqs. (32) and (34)]. First, we note that the contributions from S and Ω have identical forms, and that the integrands are positive definite[3]; see Fig. 1. Thus, as is

[3]We have found a different result for $(\eta_{yx})_u^S$ from RS06, in particular only obtaining the first part of their Eq. (D5), and are currently unsure

well known, we see that $(\eta_{yx})_u^S$, the "shear-current effect," has the incorrect sign for dynamo action within this quasilinear approximation. Although the basic $\boldsymbol{\Omega} \times \boldsymbol{J}$ effect (also known as the Rädler effect) is well known, the explicit calculation of transport coefficients including shear and rotation seems to have been mostly ignored, although there is much discussion in early literature on the subject (e.g., Krause and Rädler [2], Moffatt and Proctor [14]). Given the identical forms of Eqs. (32) and (34), we can immediately write down the result

$$(\eta_{yx})_u = (S - 2\Omega)\Xi, \tag{37}$$

where Ξ is the (positive) integral in Eq. (32). Thus, we find that the addition of Keplerian rotation ($\Omega = 2S/3$) (as relevant to turbulence in accretion disks for example) will change the sign of η_{yx} to slightly negative and a coherent dynamo instability should be possible. Indeed, this is seen in our recent simulation work [12], where we observe increasing coherency and a larger growth rate as the rotation is increased in the anticyclonic direction.

Turning to the coefficients for magnetic fluctuations we find the interesting possibility of a magnetically driven dynamo. In particular, as shown in Appendix (C) and Fig. 1, the coefficient $(\eta_{yx})_b$ is consistently negative and generally larger than the other contributions. This implies that a dynamo can be excited by magnetic fluctuations, themselves presumably arising from a small-scale dynamo process, or perhaps an MHD instability of some sort. Since the small-scale dynamo is usually considered harmful to mean fields [5], this is an interesting possibility—a buildup of magnetic noise on small scales may *cause* a coherent large-scale dynamo to develop. Interestingly, the $\boldsymbol{u}$ fluctuations that allow for this magnetic shear-current effect arise solely through the pressure response of the fluid; i.e., the ∇p term in Eq. (14). This can be seen by redoing the calculation with only the pressure response included in the $\boldsymbol{m}$ equations, which leads to identical results for $(\eta_{yx})_b$. We note that the fluid pressure is also fundamental for the vanishing of the magnetic contribution to the diagonal turbulent resistivity $(\beta_0)_b$ [Eq. (B21)], which is only zero because of an exact cancellation between a term arising through the pressure response and a term of a similar form to $(\beta^{(0)})_u$ [6]. Thus the magnetic shear-current effect is related to the well-known lack of β quenching (i.e., $(\beta^{(0)})_b = 0$), but arises in the off-diagonal resistivity due to the presence of a large-scale shear flow.

The addition of rotation renders the effect of magnetic fluctuations more complex, and no simple result seems possible. In particular, the sign of the $(\eta_{yx})_b^\Omega$ coefficient depends on the parameters, and is generally negative for large ν, η and positive at lower dissipation, although smaller in magnitude than $(\eta_{yx})_b^S$. This change in sign is also seen in quasilinear calculations [12]; however, given that the quasilinear approximation becomes less valid in this limit, it would be unwise to draw any conclusions about the high-Rm limit from this behavior.

Finally, we note the possible relevance of this dynamo to the central regions of accretion disks. In self-sustaining turbulence simulations in this geometry, magnetic fluctuations are generally substantially stronger than velocity fluctuations. Such conditions seem ideal for excitation of a coherent dynamo driven by the magnetic shear-current effect. We note that cyclic behavior, as often observed in self-sustaining simulations [4,26], seems to be quite generic in the nonlinear development of the magnetic shear-current effect, and we have observed this in low-Rm simulations with a forced induction equation [12]. In addition, it is worth noting that Lesur and Ogilvie [4] concluded that η_{yx} was the primary dynamo driver from analysis of their numerical simulations. While more work is obviously needed to explore this possibility in detail, it seems reasonable to conclude that the magnetic shear-current effect is playing a fundamental role.

V. SPECIFIC RESULTS FOR STRATIFIED ACCRETION DISKS

In this section we briefly outline how our results apply to stratified sheared rotating turbulence. Our primary motivation is consideration of the upper and lower regions of accretion disks, where the turbulence is stratified in density and intensity by the vertical gravity, perpendicular to the velocity shear. Self-sustaining turbulence simulations in this geometry (for instance with shear-periodic boundary conditions in the radial direction) exhibit a very coherent dynamo, with quasi-time-periodic behavior in B_y and B_x creating a "butterfly diagram" [24,25]. Large-scale magnetic structures are seen to emanate from the central portion of the disk, migrating upwards into the lower density regions and becoming more intense as they do so [26]. This migration behavior would be characteristic of a dynamo driven by α_{yy} above and below the midplane: as shown in Eq. (12), growth of this type of "$\alpha\omega$" dynamo is always accompanied by dynamo waves since Γ is complex. Note that a negative imaginary part of Γ is required for upwards migration of mean-field structures with $\hat{\boldsymbol{g}} = \hat{\boldsymbol{z}}$. This occurs for $a_{yy} < 0$, $a_{xy} < 0$, $(a_{yx} > 0)$ [40].

Utilizing Eq. (13) with the results listed in Appendix B, and setting Pm = 1 here for simplicity, one obtains

$$(a_{yy})_u^S = 8\pi\chi_{\rho\bar{u}} \int d\omega\, dk \frac{k^2 W_u(k,u)\tilde{\nu}^2(5\tilde{\nu}^2+\omega^2)}{15(\tilde{\nu}^2+\omega^2)^3}, \tag{38}$$

$$(a_{yy})_b^S = -4\pi\chi_{\bar{b}} \int d\omega\, dk\, \rho^{-1} W_b(k,u) k^2 \frac{7\tilde{\nu}^4 - 4\omega^2\tilde{\nu}^2 - 3\omega^4}{15(\tilde{\nu}^2+\omega^2)^3}, \tag{39}$$

$$(a_{yy})_u^\Omega = -64\pi\chi_{\rho\bar{u}} \int d\omega\, dk \frac{k^2 W_u(k,u)\tilde{\nu}^2(\tilde{\nu}^2+5\omega^2)}{15(\tilde{\nu}^2+\omega^2)^3}, \tag{40}$$

$$(a_{yy})_b^\Omega = -64\pi\chi_{\bar{b}} \int d\omega\, dk \frac{\rho^{-1} W_b(k,u) k^2 \omega^2(\omega^2 - 3\tilde{\nu}^2)}{15(\tilde{\nu}^2+\omega^2)^3}. \tag{41}$$

Finally, for the off-diagonal component, $\gamma^{(0)} = a_{xy} = -a_{yx}$, one has

$$(\gamma^{(0)})_u = 4\pi\chi_{\bar{u}} \int d\omega\, dk \frac{k^2 W_u(k,u)\tilde{\eta}}{3(\tilde{\eta}^2+\omega^2)}, \tag{42}$$

from where this discrepancy arises. We have one difference in the full transport coefficients (in the $\beta^{(D)}$ term; see Appendix B), but this difference alone does not fix the discrepancy. In any case, the main conclusion—that $(\eta_{yx})_u^S$ has the incorrect sign for dynamo action—is unchanged. Our expressions for $(\eta_{yx})_u^\Omega$ are identical.

$$(\gamma^{(0)})_b = -4\pi\chi_{\bar{b}} \int d\omega\, dk \frac{k^2\rho^{-1}W_b(k,u)\tilde{\eta}}{3(\tilde{\eta}^2+\omega^2)}. \quad (43)$$

Here we use the notation $\chi_{\rho\bar{u}} = |\nabla \ln(\rho\bar{u})|$, and again signs are defined such that

$$a_{yy} = S\left[(a_{yy})^S_u + (a_{yy})^S_b\right] + \Omega\left[(a_{yy})^\Omega_u + (a_{yy})^\Omega_b\right] \quad (44)$$

for anticyclonic rotation, e.g., Keplerian rotation is $\Omega = 2/3S$.

It is first worth noting the sign of each coefficient given in Eqs. (38)–(43). With $\chi_{\rho\bar{u}}, \chi_{\bar{b}} > 0$ it can be shown easily from the above expressions that

$$(a_{yy})^S_u > 0, \quad (a_{yy})^S_b < 0, \quad (a_{yy})^\Omega_u < 0, \quad da1(a_{yy})^\Omega_b > 0. \quad (45)$$

(Note that for the b components, it is necessary to integrate by parts over ω; see Appendix C). The relations in Eq. (45) appear to also hold for Pm $\neq 1$ (although we have a proof of this only for the Ω coefficients). This consistent difference in sign between contributions is rather inconvenient for the application of SOCA results to stratified accretion disks. Since one expects $\chi_{\rho\bar{u}} < 0$, $\chi_{\bar{b}} < 0$ (although possibly $\chi_{\bar{u}} > 0$) [25,41], we are left with the situation where not only do the α effects due to u and b partially cancel, but also those due to rotation and velocity shear! What is more, as shown in Fig. 2, the relative contribution of each depends strongly on Pm. In particular, we see a dominance of $(a_{yy})_u$ over $(a_{yy})_b$ for Pm $\gtrsim 1$, but this can reverse at low Pm. Similarly, the relative contributions due to velocity shear and rotation for the magnetic effect vary substantially with Pm, although the effect of shear seems generally more substantial. While the ratio of kinematic shear and rotation contributions may be somewhat more robust, the two are roughly equal in magnitude, $(a_{yy})^S_u \sim -(a_{yy})^\Omega_u$, and will approximately cancel for Keplerian rotation. Finally, it is worth noting that to complement these uncertainties, the signs of $\gamma^{(0)}$ seem to predict the *opposite* field migration pattern to the upwards transport seen in simulation. In particular, for $\chi_{\bar{b}} < 0$, $\chi_{\bar{u}} > 0$, the kinematic and magnetic contributions both enforce $\gamma^{(0)} > 0$, leading to Im $\Gamma > 0$. However, in our use of the anelastic approximation, buoyancy effects are not included and these would be expected to change this aspect of the calculation substantially [40,42,43], potentially through large-scale instability [44].

Where does this leave us for understanding the dynamo in stratified accretion disks? We see that aside from perhaps the transport term $\gamma^{(0)}$, claims that SOCA predictions are *incorrect* for the stratified regions of accretion disks are unfounded. More accurately, one could say that SOCA predictions themselves are completely inconclusive, even in the kinematic regime, since each contribution—kinematic, magnetic, rotation, and velocity shear—has a tendency to cancel its partner. Such uncertainty seems at odds with the robust dynamo "butterfly diagram" seen across a wide variety of accretion disk simulations.

Of course, one possibility is that the SOCA calculation carried out here, keeping only the linear contributions due to Ω, S, and stratification, is not up to the task of calculating these coefficients, and in reality there is a robust α effect. For instance, in Rüdiger and Pipin [40], the authors find that α_{yy} has the correct sign ($\alpha_{yy} < 0$) for magnetic fluctuations in a compressible turbulence model for Keplerian shear and moderate Pm [this is the sign opposite to Eq. (39) but since their effect vanishes in the incompressible limit, one should have no reason to expect agreement]. Similarly, the calculations presented in Donnelly [45] go well beyond the accuracy of SOCA for the specific case of Keplerian shear through nonperturbative inclusion of several extra physical

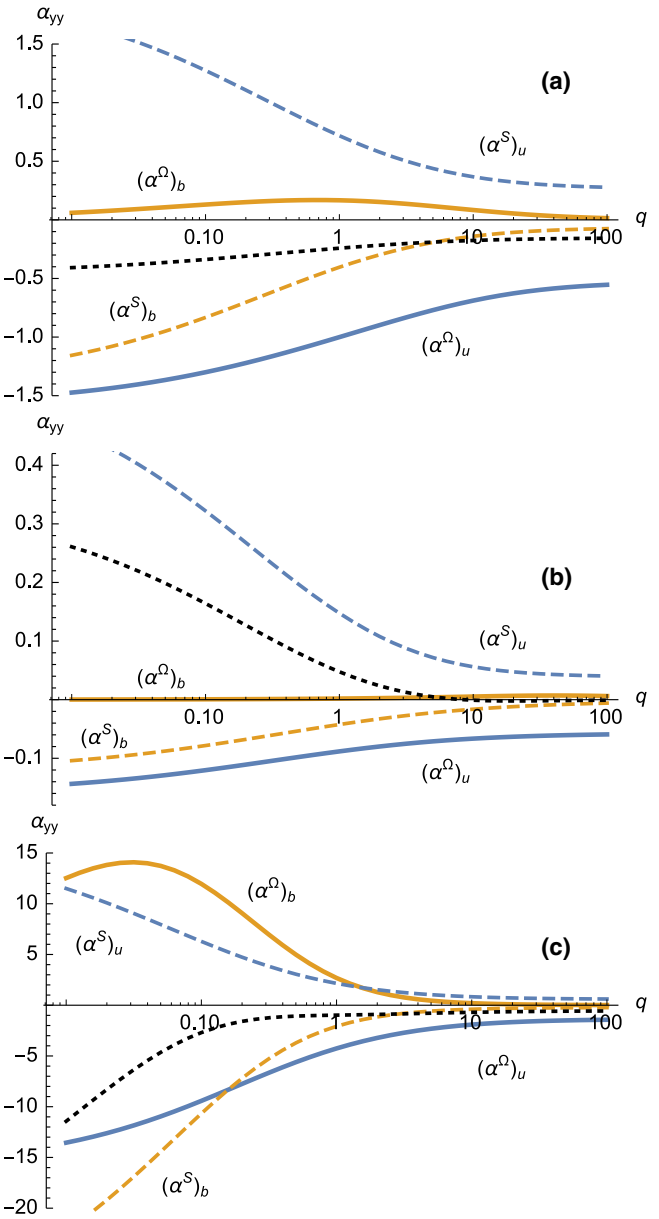

FIG. 2. (Color online) Transport coefficients $(a_{yy})^\Omega_u$ (solid, blue), $(a_{yy})^S_u$ (dashed, blue), $(a_{yy})^\Omega_b$ (solid, orange) and $(a_{yy})^S_b$ (dashed, orange) as a function of q for (a) Pm $= 1$, (b) Pm $= 10$, and (c) Pm $= 1/10$ (lines also labeled on each plot). Each coefficient has been calculated using the form given in Eq. 30 for W, and normalized by $(\beta^{(0)})_u$ with the magnetic diffusion time, λ_c^2/η, held constant (equivalently $\tau_c = 1/q$). The dotted (black) curve in each plot shows the total a_{yy} with equal kinetic and magnetic turbulence levels for Keplerian rotation, $\Omega = 2/3S$ [Eq. (44)], to illustrate the variability in these predictions.

effects; however, it is unclear from their (rather complicated) expressions whether the theory predicts a specific sign for α_{yy}. While certainly feasible, it would seem a little bizarre that a behavior that appears so robustly in simulation could show so much variability across different calculation methods or rely on nonlinear behavior of transport coefficients with Ω, S, or the stratification. In addition, recent (quasikinematic) test-field calculations in self-sustaining stratified turbulence [46] have shown α_{yy} to be robustly positive, although interestingly the dynamo period (as a function of S) nicely matches that inferred from $|\alpha_{yy}|$.

A variety of other mechanisms to create a butterfly diagram are imaginable, for instance a dynamo driven primarily by the magnetic shear-current effect up to relatively far from the midplane (Sec. IV), with upwards transport above this caused by large-scale buoyant instability (not included here due to the anelastic approximation). Another possibility could be that upwards field transport is caused by a small-scale magnetic helicity flux [47,48] from the central shear-current dynamo, which would create a (helical) magnetic α effect. Such a process could look rather similar to a more standard α effect, although the basic cause of the dynamo would be entirely different [25]. Note that magnetic helicity fluxes have been found to play a significant role in unstratified global MRI turbulence [49], providing some indication that such a process could be important. It is also worth noting that spatial variation in transport coefficients and quenching can lead to some interesting possibilities for dynamo action [50,51], and similar effects may prove important at the boundary between the stratified and unstratified regions of disks. Overall, it seems that the underlying cause for the "butterfly diagram" in stratified disks remains unclear and more work will be needed to arrive at robust mean-field models of the process.

VI. DISCUSSION AND CONCLUSIONS

In this work we have theoretically studied the dynamo in systems with mean velocity gradients, rotation, net helicity, and stratification, using perturbative calculations within the second-order correlation approximation. In addition to the standard kinematic dynamo, we have considered the possibility of a dynamo driven by small-scale *magnetic fluctuations,* as might arise from the small-scale dynamo or an instability. Our main finding is that an off-diagonal resistivity coupled to the shear can cause a dynamo instability in the presence of magnetic fluctuations. This effect—the magnetic analog of the "shear-current effect" [9,17]—raises the interesting possibility of the small-scale dynamo *enhancing* the growth of a large-scale field. In some sense, this possibility is the reverse of large-scale quenching [5,27]; rather than the small-scale magnetic fluctuations inhibiting the large-scale field growth, they could actively aid field generation, with large-scale growth eventually halting due to nonlinear changes to the transport coefficients, possibly influenced by secondary quenching effects [52].

Importantly, our prediction that the magnetic shear-current effect is able to excite a dynamo agrees with other transport coefficient calculation methods and simulations. In particular, the τ approximation predicts the linear magnetic effect to be much stronger than the kinematic effect (see Fig. 3 of Rogachevskii and Kleeorin [9]), just as was found in this work using SOCA (Fig. 1). In addition, agreement is found with quasilinear calculations [12] (the magnetic version of the calculations in Singh and Sridhar [21]), as well as perturbative inhomogeneous shearing wave calculations [22]. This suggests that the effect may be more robust than the kinematic shear-current effect and/or have less dependence on Reynolds numbers.

The work presented in this article was primarily motivated by gaining improved understanding of the fundamental dynamo mechanisms in accretion disks. Consistent with the idea that two dynamo mechanisms might operate in disks [53], their inner regions seem well suited to be explained by the magnetic shear-current effect [4]—magnetic fluctuations are generally stronger than kinetic fluctuations, rotation has the correct sign to enhance the kinematic dynamo, and the turbulence is essentially unstratified and nonhelical. Concurrent nonlinear direct numerical simulations of unstratified shear dynamos in Cartesian boxes [12,13] have confirmed all results discussed in Sec. IV for the low-Rm regime [12,54]. First, we see a qualitative change in the kinematic dynamo with the addition of rotation, due to the change in sign of the η_{yx} transport coefficient [12]. Second, we observe the magnetically driven shear-current effect, both through direct driving of the induction equation [12], and at higher magnetic Reynolds number where magnetic fluctuations arise self-consistently though excitation of a small-scale dynamo [13]. The nonlinear saturation of these magnetically driven large-scale dynamos exhibits a pleasing resemblance to self-sustaining unstratified accretion disk turbulence simulations, with quasicyclic behavior of the large-scale B_y field.

Less clear have been our findings regarding the α effect, as relevant to the stratified regions of accretion disks. In particular, we find that α coefficients arising from rotation and shear, and those arising from kinetic and magnetic fluctuations, are each of opposite signs for anticyclonic rotation ($\boldsymbol{\Omega}$ and $\boldsymbol{\nabla} \times \boldsymbol{U}$ antiparallel), and thus would tend to cancel. Furthermore, predictions about which of these terms dominate (thus determining the sign of the total α effect), depend strongly on the magnetic Prandtl number and the relative levels of kinetic and magnetic turbulence. We thus conclude that perturbative SOCA calculations *give no useful predictions* regarding the primary driver of the so-called "butterfly diagram" pattern of large-scale field evolution seen in self-sustaining stratified accretion disk simulations. Whether this is simply due to the inaccuracies of SOCA or there is some other more exotic effect operating (e.g., a helicity flux [49]) remains to be seen.

ACKNOWLEDGMENTS

This work was supported by a Procter Fellowship at Princeton University and U.S. Department of Energy Grant No. DE-AC02-09-CH11466. The authors would like to thank I. Rogachevskii, A. Schekochihin, and J. Krommes for enlightening discussion and useful suggestions.

APPENDIX A: EQUATIONS FOR $u^{(0)}$, $u^{(1)}$, $b^{(0)}$, $b^{(1)}$ IN FOURIER SPACE

Here we give the set of perturbation equations for $\boldsymbol{u}$ and $\boldsymbol{b}$ in Fourier space, as result from the Fourier transform of Eq. (14). The method is outlined in RS06, so we give very little detail here. Since we assume $U_i(\boldsymbol{x}) = U_{ij}x_j$, $\rho = \rho_0 + \chi_\rho \hat{g}_i x_i$, and $B_i(\boldsymbol{x}) = B_i + B_{ij}x_j$ the Fourier transforms can be carried out exactly using $\widehat{x_k \partial_l b_j} = -\delta_{lk}\hat{b}_j - k_l \partial_{k_k}\hat{b}_j$ (where $\hat{\cdot}$ denotes the Fourier transform). We have also neglected products of χ_ρ with B_{ij}. In the momentum equations, the projection operator $\delta_{ij} - k_i k_j/k^2$ is applied so as to remove the pressure.

Defining, as in RS06,

$$N_\nu = \frac{1}{i\omega - \nu k^2}, \quad E_\eta = \frac{1}{i\omega - \eta k^2}, \tag{A1}$$

the Fourier space equations are as follows:

$$m_i^{(0)} = N_\nu\Big[-U_{il}m_{0l} + U_{lk}k_l\frac{\partial m_{0i}}{\partial k_k} + 2\frac{k_i k_j}{k^2}m_{0l}U_{jl} - i\nu k_r\chi_\rho\hat{g}_r m_{0i} + i\nu\frac{k_i k_j k_r}{k^2}\chi_\rho\hat{g}_r m_{0j} + 2\frac{k_r\Omega_r}{k^2}\varepsilon_{ijk}m_{0j}k_k + ik_r B_r b_{0i}$$
$$-ik_r B_r\frac{k_i k_j}{k^2}b_{0j} + B_{il}b_{0l} - B_{lk}k_l\frac{\partial b_{0i}}{\partial k_k} - 2\frac{k_i k_j}{k^2}b_{0l}B_{jl}\Big], \tag{A2}$$

$$m_i^{(1)} = N_\nu\Big[-U_{il}m_l^{(0)} + U_{lk}k_l\frac{\partial m_i^{(0)}}{\partial k_k} + 2\frac{k_i k_j}{k^2}m_l^{(0)}U_{jl} - i\nu k_r\chi_\rho\hat{g}_r m_i^{(0)} + i\nu\frac{k_i k_j k_r}{k^2}\chi_\rho\hat{g}_r m_j^{(0)} + 2\frac{k_r\Omega_r}{k^2}\varepsilon_{ijk}m_j^{(0)}k_k + ik_r B_r b_i^{(0)}$$
$$-ik_r B_r\frac{k_i k_j}{k^2}b_j^{(0)} + B_{il}b_l^{(0)} - B_{lk}k_l\frac{\partial b_i^{(0)}}{\partial k_k} - 2\frac{k_i k_j}{k^2}b_l^{(0)}B_{jl}\Big], \tag{A3}$$

$$b_i^{(0)} = E_\eta\Big[\rho_0^{-1}\Big(ik_r B_r m_{0i} - B_{ij}m_{0j} - B_{jk}k_j\frac{\partial m_{0i}}{\partial k_k} + B_i\chi_\rho\hat{g}_r m_{0r} + \chi_\rho\hat{g}_r B_j k_j\frac{\partial m_{0i}}{\partial k_r}\Big) + U_{ij}b_{0j} + U_{jk}k_j\frac{\partial b_{0i}}{\partial k_k}\Big], \tag{A4}$$

$$b_i^{(1)} = E_\eta\Big[\rho_0^{-1}\Big(ik_r B_r m_i^{(0)} - B_{ij}m_j^{(0)} - B_{jk}k_j\frac{\partial m_i^{(0)}}{\partial k_k} + B_i\chi_\rho\hat{g}_r m_r^{(0)} + \chi_\rho\hat{g}_r B_j k_j\frac{\partial m_i^{(0)}}{\partial k_r}\Big) + U_{ij}b_j^{(0)} + U_{jk}k_j\frac{\partial b_i^{(0)}}{\partial k_k}\Big]. \tag{A5}$$

Here m_{0i}, b_{0i}, etc., refer to the Fourier space variables for simplicity of notation. As a first step in the calculation, Eqs. (A2) and (A4) are inserted into Eqs. (A3) and (A5) and expanded, neglecting those terms that contain $U_{ij}U_{rs}$, $U_{ij}\Omega_r$, $\Omega_i\Omega_j$, $U_{ij}\,\chi_\rho$, $\Omega\,\chi_\rho$, χ_ρ^2, $B_i B_j$, $B_i B_{ij}$, and $B_{ij}B_{rs}$ as higher order in this perturbation expansion.

APPENDIX B: LIST OF ALL TRANSPORT COEFFICIENTS

In this Appendix we list all transport coefficients $\alpha^{(0)}\beta^{(0)}$, $\delta^{(\Omega)}$, ... in the form of integrals over the isotropic velocity and magnetic correlation functions, $W_u(\boldsymbol{R},k,\omega)$, $H_u(k,\omega)$, $W_b(\boldsymbol{R},k,\omega)$, $H_b(k,\omega)$. This parallels Appendix B in RS06 and there is some overlap; however, for completeness we list all coefficients.

Analogous to the relations in Sec. IV for the Cartesian case and RS06, we list here the coefficient of $4\pi k^2 W_{u,b}$ or $4\pi k^2 H_{u,b}$ in the integrand of each transport coefficient; that is $\tilde{\alpha}_H^{(\cdot)}$, $\tilde{\alpha}^{(\cdot)}$ or $\tilde{\beta}^{(\cdot)}$ in

$$\big(\alpha_H^{(\cdot)}\big)_{u,b} = 4\pi\int dk\,d\omega\,k^2\tilde{\alpha}_H^{(\cdot)}(k,\omega)H_{u,b}(k,\omega), \quad \big(\alpha^{(\cdot)}\big)_{u,b} = 4\pi\int dk\,d\omega\,k^2\tilde{\alpha}^{(\cdot)}(k,\omega)W_{u,b}(k,\omega),$$
$$(\beta^{(\cdot)})_{u,b} = 4\pi\int dk\,d\omega\,k^2\tilde{\beta}^{(\cdot)}(k,\omega)W_{u,b}(k,\omega). \tag{B1}$$

We use the notation $\tilde{\eta} = k^2\eta$, $\tilde{\nu} = k^2\nu$, and $\boldsymbol{\nabla}\ln a \equiv \chi_a\,\hat{\boldsymbol{g}}$ (e.g., $\boldsymbol{\nabla}\ln\rho + \boldsymbol{\nabla}\ln\bar{u} = \chi_{\rho\bar{u}}\,\hat{\boldsymbol{g}}$).

1. Nonhelical α coefficients

$$(\gamma^{(0)})_u = \frac{\chi_{\bar{u}}\tilde{\eta}}{6(\tilde{\eta}^2+\omega^2)}, \tag{B2}$$

$$(\gamma^{(0)})_b = -\frac{\chi_{\bar{b}}\tilde{\nu}}{6\rho(\tilde{\nu}^2+\omega^2)}, \tag{B3}$$

$$(\gamma^{(\Omega)})_u = -\frac{\chi_{\rho\bar{u}}\omega^2}{3(\tilde{\eta}^2+\omega^2)(\tilde{\nu}^2+\omega^2)}, \tag{B4}$$

$$(\gamma^{(\Omega)})_b = \frac{\chi_{\bar{b}}(\omega^2-\tilde{\nu}^2)}{6\rho(\tilde{\nu}^2+\omega^2)^2}, \tag{B5}$$

$$\left(\alpha_1^{(\Omega)}\right)_u = \frac{4\chi_{\rho\bar{u}}\tilde{\eta}[2\omega^2\tilde{\eta}(\tilde{\nu}^2+\omega^2)+\tilde{\eta}^2(3\omega^2\tilde{\nu}+\tilde{\nu}^3)+\omega^2\tilde{\nu}(\tilde{\nu}^2+3\omega^2)]}{15(\tilde{\eta}^2+\omega^2)^2(\tilde{\nu}^2+\omega^2)^2}, \tag{B6}$$

$$\left(\alpha_1^{(\Omega)}\right)_b = \frac{4\chi_{\bar{b}}\omega^2(\omega^2-3\tilde{\nu}^2)}{15\rho(\tilde{\nu}^2+\omega^2)^3}, \tag{B7}$$

$$\left(\alpha_2^{(\Omega)}\right)_u = \frac{\chi_{\rho\bar{u}}}{15}[2\omega^2\tilde{\eta}\tilde{\nu}(\omega^2-3\tilde{\nu}^2)+3\omega^2\tilde{\eta}^2(\tilde{\nu}^2+\omega^2)+2\tilde{\eta}^3\tilde{\nu}(\omega^2-3\tilde{\nu}^2)-5\omega^4(\tilde{\nu}^2+\omega^2)](\tilde{\eta}^2+\omega^2)^{-2}(\tilde{\nu}^2+\omega^2)^{-2}, \tag{B8}$$

$$\left(\alpha_2^{(\Omega)}\right)_b = \frac{\chi_{\bar{b}}(3\omega^4-24\omega^2\tilde{\nu}^2+5\tilde{\nu}^4)}{30\rho(\tilde{\nu}^2+\omega^2)^3}, \tag{B9}$$

$$\begin{aligned}\left(\alpha_1^{(W)}\right)_u = \frac{\chi_{\rho\bar{u}}}{120}&[4\tilde{\eta}^5(11\omega^2\tilde{\nu}+5\tilde{\nu}^3)+4\tilde{\eta}(11\omega^6\tilde{\nu}+5\omega^4\tilde{\nu}^3)+8\tilde{\eta}^3(11\omega^4\tilde{\nu}+5\omega^2\tilde{\nu}^3)+\tilde{\eta}^4(12\omega^2\tilde{\nu}^2-\tilde{\nu}^4+13\omega^4)\\&-4\tilde{\eta}^2(5\omega^4\tilde{\nu}^2+3\omega^2\tilde{\nu}^4+2\omega^6)+5\omega^4\tilde{\nu}^4-5\omega^8](\tilde{\eta}^2+\omega^2)^{-3}(\tilde{\nu}^2+\omega^2)^{-2},\end{aligned} \tag{B10}$$

$$\begin{aligned}\left(\alpha_1^{(W)}\right)_b = \frac{\chi_{\bar{b}}}{120}&[4\omega^2\tilde{\eta}\tilde{\nu}(\tilde{\nu}^2+\omega^2)^2+\tilde{\eta}^4(\tilde{\nu}^4-36\omega^2\tilde{\nu}^2+11\omega^4)-4\tilde{\eta}^3\tilde{\nu}(\tilde{\nu}^2+\omega^2)^2+4\tilde{\eta}^2(-11\omega^4\tilde{\nu}^2+5\omega^2\tilde{\nu}^4+8\omega^6)\\&-8\omega^6\tilde{\nu}^2+19\omega^4\tilde{\nu}^4+21\omega^8](\tilde{\eta}^2+\omega^2)^{-2}(\tilde{\nu}^2+\omega^2)^{-3}\rho^{-1},\end{aligned} \tag{B11}$$

$$\begin{aligned}\left(\alpha_2^{(W)}\right)_u = \frac{\chi_{\rho\bar{u}}}{240}&[-4\tilde{\eta}^5(3\omega^2\tilde{\nu}+5\tilde{\nu}^3)-4\tilde{\eta}(3\omega^6\tilde{\nu}+5\omega^4\tilde{\nu}^3)+\tilde{\eta}^4(44\omega^2\tilde{\nu}^2+13\tilde{\nu}^4+31\omega^4)-8\tilde{\eta}^3(3\omega^4\tilde{\nu}+5\omega^2\tilde{\nu}^3)\\&-28\tilde{\eta}^2(5\omega^4\tilde{\nu}^2+3\omega^2\tilde{\nu}^4+2\omega^6)+5(8\omega^6\tilde{\nu}^2+3\omega^4\tilde{\nu}^4+5\omega^8)](\tilde{\eta}^2+\omega^2)^{-3}(\tilde{\nu}^2+\omega^2)^{-2},\end{aligned} \tag{B12}$$

$$\begin{aligned}\left(\alpha_2^{(W)}\right)_b = \frac{\chi_{\bar{b}}}{240}&[28\omega^2\tilde{\eta}\tilde{\nu}(\tilde{\nu}^2+\omega^2)^2-28\tilde{\eta}^3\tilde{\nu}(\tilde{\nu}^2+\omega^2)^2+\tilde{\eta}^4(-12\omega^2\tilde{\nu}^2+7\tilde{\nu}^4-3\omega^4)-4\tilde{\eta}^2(17\omega^4\tilde{\nu}^2-5\omega^2\tilde{\nu}^4+14\omega^6)\\&-56\omega^6\tilde{\nu}^2+13\omega^4\tilde{\nu}^4-53\omega^8](\tilde{\eta}^2+\omega^2)^{-2}(\tilde{\nu}^2+\omega^2)^{-3}\rho^{-1},\end{aligned} \tag{B13}$$

$$\begin{aligned}(\alpha^{(D)})_u = \frac{\chi_{\rho\bar{u}}}{120}&[12\omega^2\tilde{\eta}^2\tilde{\nu}^2(\tilde{\nu}^2+\omega^2)+12\tilde{\eta}^5\tilde{\nu}(\omega^2-\tilde{\nu}^2)+4\omega^4\tilde{\eta}\tilde{\nu}(\tilde{\nu}^2+7\omega^2)+8\tilde{\eta}^3(5\omega^4\tilde{\nu}-\omega^2\tilde{\nu}^3)+5\omega^4\tilde{\nu}^4-5\omega^8\\&-\tilde{\eta}^4(20\omega^2\tilde{\nu}^2+9\tilde{\nu}^4+11\omega^4)](\tilde{\eta}^2+\omega^2)^{-3}(\tilde{\nu}^2+\omega^2)^{-2},\end{aligned} \tag{B14}$$

$$\begin{aligned}(\alpha^{(D)})_b = \frac{\chi_{\bar{b}}}{120}&[-4\omega^2\tilde{\eta}\tilde{\nu}(6\omega^2\tilde{\nu}^2+\tilde{\nu}^4+5\omega^4)-\tilde{\eta}^4(12\omega^2\tilde{\nu}^2-5\tilde{\nu}^4+\omega^4)+4\tilde{\eta}^3\tilde{\nu}(6\omega^2\tilde{\nu}^2+5\tilde{\nu}^4+\omega^4)\\&+4\tilde{\eta}^2(-3\omega^4\tilde{\nu}^2+3\omega^2\tilde{\nu}^4+2\omega^6)+7\omega^4\tilde{\nu}^4+9\omega^8](\tilde{\eta}^2+\omega^2)^{-2}(\tilde{\nu}^2+\omega^2)^{-3}\rho^{-1},\end{aligned} \tag{B15}$$

$$\begin{aligned}(\gamma^{(W)})_u = -\frac{\chi_{\rho\bar{u}}}{120}&[-8\omega^6\tilde{\eta}\tilde{\nu}-16\omega^4\tilde{\eta}^3\tilde{\nu}-8\omega^2\tilde{\eta}^5\tilde{\nu}-\tilde{\eta}^4(8\omega^2\tilde{\nu}^2+\tilde{\nu}^4+7\omega^4)-4\tilde{\eta}^2(7\omega^4\tilde{\nu}^2+3\omega^2\tilde{\nu}^4+4\omega^6)\\&+12\omega^6\tilde{\nu}^2+5\omega^4\tilde{\nu}^4+7\omega^8](\tilde{\eta}^2+\omega^2)^{-3}(\tilde{\nu}^2+\omega^2)^{-2},\end{aligned} \tag{B16}$$

$$\begin{aligned}(\gamma^{(W)})_b = \frac{\chi_{\bar{b}}}{120}&[4\tilde{\eta}^2(-3\omega^4\tilde{\nu}^2+2\omega^2\tilde{\nu}^4+3\omega^6)-8\omega^2\tilde{\eta}\tilde{\nu}(\tilde{\nu}^2+\omega^2)^2+\tilde{\eta}^4(-12\omega^2\tilde{\nu}^2+3\tilde{\nu}^4+\omega^4)\\&+5\omega^4\tilde{\nu}^4+11\omega^8](\tilde{\eta}^2+\omega^2)^{-2}(\tilde{\nu}^2+\omega^2)^{-3}\rho^{-1},\end{aligned} \tag{B17}$$

$$\begin{aligned}(\gamma^{(D)})_u = -\frac{\chi_{\rho\bar{u}}}{120}&[9\tilde{\eta}^4(\omega^4-\tilde{\nu}^4)+8\tilde{\eta}^5(5\omega^2\tilde{\nu}+6\tilde{\nu}^3)+8\tilde{\eta}(3\omega^6\tilde{\nu}+4\omega^4\tilde{\nu}^3)+16\tilde{\eta}^3(4\omega^4\tilde{\nu}+5\omega^2\tilde{\nu}^3)\\&+4\tilde{\eta}^2(13\omega^4\tilde{\nu}^2+3\omega^2\tilde{\nu}^4+10\omega^6)+5\omega^4(4\omega^2\tilde{\nu}^2+\tilde{\nu}^4+3\omega^4)](\tilde{\eta}^2+\omega^2)^{-3}(\tilde{\nu}^2+\omega^2)^{-2},\end{aligned} \tag{B18}$$

$$\begin{aligned}(\gamma^{(D)})_b = \frac{\chi_{\bar{b}}}{120}&[-16\omega^2\tilde{\eta}\tilde{\nu}(3\omega^2\tilde{\nu}^2+\tilde{\nu}^4+2\omega^4)+\tilde{\eta}^4(12\omega^2\tilde{\nu}^2+19\tilde{\nu}^4-23\omega^4)-8\tilde{\eta}^3(3\omega^4\tilde{\nu}+4\omega^2\tilde{\nu}^3+\tilde{\nu}^5)\\&+\tilde{\eta}^2(52\omega^4\tilde{\nu}^2+56\omega^2\tilde{\nu}^4-36\omega^6)+40\omega^6\tilde{\nu}^2+37\omega^4\tilde{\nu}^4-13\omega^8](\tilde{\eta}^2+\omega^2)^{-2}(\tilde{\nu}^2+\omega^2)^{-3}\rho^{-1}.\end{aligned} \tag{B19}$$

2. β coefficients

$$(\beta^{(0)})_u = \frac{\tilde{\eta}}{3(\tilde{\eta}^2+\omega^2)}, \tag{B20}$$

$$(\beta^{(0)})_b = 0, \tag{B21}$$

$$(\delta^{(\Omega)})_u = -\frac{\omega^2}{3(\tilde{\eta}^2+\omega^2)(\tilde{\nu}^2+\omega^2)}, \tag{B22}$$

$$(\delta^{(\Omega)})_b = \frac{\tilde{\nu}^2-\omega^2}{6\rho(\tilde{\nu}^2+\omega^2)^2}, \tag{B23}$$

$$(\delta^{(W)})_u = \frac{\tilde{\eta}^2 - \omega^2}{12(\tilde{\eta}^2 + \omega^2)^2}, \tag{B24}$$

$$(\delta^{(W)})_b = \frac{\tilde{\nu}^2 - \omega^2}{12\rho(\tilde{\nu}^2 + \omega^2)^2}, \tag{B25}$$

$$(\kappa^{(\Omega)})_u = \frac{2\omega^2(11\tilde{\eta}^2 - 5\omega^2)}{15(\tilde{\eta}^2 + \omega^2)^2(\tilde{\nu}^2 + \omega^2)}, \tag{B26}$$

$$(\kappa^{(\Omega)})_b = \frac{9\tilde{\nu}^4 - 48\omega^2\tilde{\nu}^2 + 7\omega^4}{15\rho(\tilde{\nu}^2 + \omega^2)^3}, \tag{B27}$$

$$(\kappa^{(W)})_u = \frac{\tilde{\eta}^4(23\omega^2 - \tilde{\nu}^2) + 12\tilde{\eta}^2(\omega^4 - \omega^2\tilde{\nu}^2) + 5\omega^4(\tilde{\nu}^2 + \omega^2)}{30(\tilde{\eta}^2 + \omega^2)^3(\tilde{\nu}^2 + \omega^2)}, \tag{B28}$$

$$(\kappa^{(W)})_b = \frac{3\tilde{\eta}^2(-12\omega^2\tilde{\nu}^2 + \tilde{\nu}^4 + 3\omega^4) - 20\omega^4\tilde{\nu}^2 + 15\omega^2\tilde{\nu}^4 + 13\omega^6}{30\rho(\tilde{\eta}^2 + \omega^2)(\tilde{\nu}^2 + \omega^2)^3}, \tag{B29}$$

$$\begin{aligned}(\beta^{(D)})_u = \frac{1}{30}[&2\tilde{\eta}^5\tilde{\nu}(5\tilde{\nu}^2 + \omega^2) + 16\omega^2\tilde{\eta}^3\tilde{\nu}^3 + 5\omega^4(\tilde{\nu}^2 + \omega^2)^2 + \tilde{\eta}(6\omega^4\tilde{\nu}^3 - 2\omega^6\tilde{\nu}) - \tilde{\eta}^4(10\omega^2\tilde{\nu}^2 + 3\tilde{\nu}^4 + 7\omega^4)\\ &-2\tilde{\eta}^2(8\omega^4\tilde{\nu}^2 + 3\omega^2\tilde{\nu}^4 + 5\omega^6)](\tilde{\eta}^2 + \omega^2)^{-3}(\tilde{\nu}^2 + \omega^2)^{-2},\end{aligned} \tag{B30}$$

$$\begin{aligned}(\beta^{(D)})_b = \frac{1}{10}[&4\tilde{\eta}^3\tilde{\nu}^3(\tilde{\nu}^2 + \omega^2) + 4\tilde{\eta}^2(\omega^6 - 3\omega^4\tilde{\nu}^2) - 4\omega^2\tilde{\eta}\tilde{\nu}(3\omega^2\tilde{\nu}^2 + \tilde{\nu}^4 + 2\omega^4) - 6\omega^6\tilde{\nu}^2 - \omega^4\tilde{\nu}^4 + 3\omega^8\\ &+\tilde{\eta}^4(-6\omega^2\tilde{\nu}^2 + \tilde{\nu}^4 + \omega^4)](\tilde{\eta}^2 + \omega^2)^{-2}(\tilde{\nu}^2 + \omega^2)^{-3}\rho^{-1},\end{aligned} \tag{B31}$$

$$\begin{aligned}(\kappa^{(D)})_u = \frac{1}{30}[&2\tilde{\eta}^5\tilde{\nu}(5\tilde{\nu}^2 + \omega^2) + 16\omega^2\tilde{\eta}^3\tilde{\nu}^3 + \tilde{\eta}(6\omega^4\tilde{\nu}^3 - 2\omega^6\tilde{\nu}) + \tilde{\eta}^4(10\omega^2\tilde{\nu}^2 + 3\tilde{\nu}^4 + 7\omega^4) + 2\tilde{\eta}^2(8\omega^4\tilde{\nu}^2 + 3\omega^2\tilde{\nu}^4 + 5\omega^6)\\ &-5\omega^4(\tilde{\nu}^2 + \omega^2)^2](\tilde{\eta}^2 + \omega^2)^{-3}(\tilde{\nu}^2 + \omega^2)^{-2},\end{aligned} \tag{B32}$$

$$\begin{aligned}(\kappa^{(D)})_b = \frac{1}{30}[&-4\tilde{\eta}^3\tilde{\nu}^3(\tilde{\nu}^2 + \omega^2) + 4\omega^2\tilde{\eta}\tilde{\nu}(3\omega^2\tilde{\nu}^2 + \tilde{\nu}^4 + 2\omega^4) + \tilde{\eta}^4(-6\omega^2\tilde{\nu}^2 - 3\tilde{\nu}^4 + 5\omega^4) + 4\tilde{\eta}^2(-7\omega^4\tilde{\nu}^2 - 4\omega^2\tilde{\nu}^4 + \omega^6)\\ &-\omega^4(22\omega^2\tilde{\nu}^2 + 13\tilde{\nu}^4 + \omega^4)](\tilde{\eta}^2 + \omega^2)^{-2}(\tilde{\nu}^2 + \omega^2)^{-3}\rho^{-1}.\end{aligned} \tag{B33}$$

3. Helical α coefficients

$$\left(\tilde{\alpha}_H^{(0)}\right)_u = \frac{2\tilde{\eta}}{3(\tilde{\eta}^2 + \omega^2)}, \tag{B34}$$

$$\left(\alpha_H^{(0)}\right)_b = -\frac{2\tilde{\nu}}{3\rho(\tilde{\nu}^2 + \omega^2)}, \tag{B35}$$

$$(\gamma^{(\Omega)})_u = 0, \tag{B36}$$

$$(\gamma^{(\Omega)})_b = 0, \tag{B37}$$

$$\left(\gamma_H^{(W)}\right)_u = \frac{\tilde{\eta}^2(\tilde{\nu}^2 + 3\omega^2) - \omega^2\tilde{\nu}^2 + \omega^4}{6(\tilde{\eta}^2 + \omega^2)^2(\tilde{\nu}^2 + \omega^2)}, \tag{B38}$$

$$\left(\gamma_H^{(W)}\right)_b = \frac{\tilde{\eta}^2(\omega^2 - \tilde{\nu}^2) - \omega^2(3\tilde{\nu}^2 + \omega^2)}{6\rho(\tilde{\eta}^2 + \omega^2)(\tilde{\nu}^2 + \omega^2)^2}, \tag{B39}$$

$$\begin{aligned}\left(\alpha_H^{(D)}\right)_u = -\frac{1}{15}[&3\tilde{\eta}^4(\omega^4 - \tilde{\nu}^4) + 4\tilde{\eta}^5(5\omega^2\tilde{\nu} - 3\tilde{\nu}^3) - 8\omega^2\tilde{\eta}^3\tilde{\nu}(\tilde{\nu}^2 - 7\omega^2) + 4\omega^4\tilde{\eta}\tilde{\nu}(\tilde{\nu}^2 + 9\omega^2)\\ &+4\tilde{\eta}^2(11\omega^4\tilde{\nu}^2 + 6\omega^2\tilde{\nu}^4 + 5\omega^6) - 5\omega^4(4\omega^2\tilde{\nu}^2 + \tilde{\nu}^4 + 3\omega^4)](\tilde{\eta}^2 + \omega^2)^{-3}(\tilde{\nu}^2 + \omega^2)^{-2},\end{aligned} \tag{B40}$$

$$\begin{aligned}\left(\alpha_H^{(D)}\right)_b = -\frac{1}{15\rho}[&\tilde{\eta}^4(-24\omega^2\tilde{\nu}^2 + 7\tilde{\nu}^4 + \omega^4) - 4\tilde{\eta}^3(3\omega^4\tilde{\nu} + 2\omega^2\tilde{\nu}^3 - \tilde{\nu}^5) + 4\tilde{\eta}^2(-11\omega^4\tilde{\nu}^2 + 2\omega^2\tilde{\nu}^4 + 3\omega^6)\\ &-4\tilde{\eta}(11\omega^6\tilde{\nu} + 18\omega^4\tilde{\nu}^3 + 7\omega^2\tilde{\nu}^5) + \omega^4(-20\omega^2\tilde{\nu}^2 + \tilde{\nu}^4 + 11\omega^4)](\tilde{\eta}^2 + \omega^2)^{-2}(\tilde{\nu}^2 + \omega^2)^{-3}.\end{aligned} \tag{B41}$$

All of the listed kinematic transport coefficients agree with those given in RS06, with one exception. This is the $(\beta^{(D)})_u$ coefficient, which contains a factor $1/30$, rather than $1/60$.

APPENDIX C: THE SIGN OF $(\eta_{yx})_b^S$

In this Appendix we argue that the sign of $(\eta_{yx})_b^S$ is always negative, given reasonable assumptions about the form of $W_b(k,\omega)$. We have not been able to find a general proof that this is the case due to the complexity of the expression Eq. (33), but instead analyze the cases $\mathrm{Pm} = 1$, $\mathrm{Pm} \ll 1$, and $\mathrm{Pm} \gg 1$ separately. In addition, plotting $(\eta_{yx})_b^S$ for Gaussian W_b [Eq. (30)] across a range of Pm (e.g., Fig. 1) leads us to the same conclusion for this specific W_b. [Note that $(\eta_{yx})_b^S$ depends nontrivially only on Pm and q when written in the dimensionless variables given in Eq. (31), meaning it is straightforward to observe positivity by plotting $(\eta_{yx})_b^S$ against q over a range of Pm.]

1. Pm = 1

Inserting $\nu = \eta$ into Eq. (33) leads to

$$(\eta_{yx})_b^S = \int d\omega\, dk\, k^2 W_b(k,\omega) \frac{8\pi(\omega^2 - \tilde{\eta}^2)(3\tilde{\eta}^2 + \omega^2)}{15(\tilde{\eta}^2 + \omega^2)^3}. \tag{C1}$$

An integration by parts in ω yields

$$(\eta_{yx})_b^S = \frac{4\pi}{15} \int d\omega\, dk \left[\frac{1}{\eta} \tan^{-1}\left(\frac{\omega}{\tilde{\eta}}\right) \frac{dW_b}{d\omega} + \frac{5\tilde{\eta}^2 + 3\omega^2}{(\tilde{\eta}^2 + \omega^2)^2} \omega \frac{dW_b}{d\omega} \right]. \tag{C2}$$

Under the reasonable assumptions that $\omega\, dW/d\omega \leqslant 0$ and $\tan^{-1}(\omega) dW/d\omega \leqslant 0$, each term in the integral must be negative. [Note that the $\tan^{-1}(\omega) dW/d\omega \leqslant 0$ condition, although it may appear less familiar, is just as restrictive as $\omega\, dW/d\omega \leqslant 0$, given the odd nature of the $\tan^{-1}$ function.]

2. Pm ≪ 1

Inserting $\eta = \nu/\mathrm{Pm}$ into Eq. (33), we carry out a series expansion about $\mathrm{Pm}^{-1} = \infty$ of the resulting expression. The reason for this expansion (rather than the more obvious expansion about $\mathrm{Pm} = 0$) is that we wish to explore that low Pm limit with large η rather than that with $\nu \to 0$, since SOCA loses applicability as $\nu, \eta \to 0$. The series expansion to first order in $1/\mathrm{Pm}^{-1}$ is

$$(\eta_{yx})_b^S \approx -\frac{8\pi}{15} \int d\omega dk\, W_b k^2 \left(\frac{3\omega^2 \tilde{\nu}^2 \tilde{\nu}^4 - 2\omega^4}{\left(\tilde{\nu}^2 + \omega^2\right)^3} \right. \tag{C3}$$

$$\left. + \frac{4\tilde{\nu}^2}{15(\tilde{\nu}^2 + \omega^2)^2} \frac{1}{\mathrm{Pm}^{-1}} + \ldots \right). \tag{C4}$$

The first term is independent of Pm, persisting as $\eta \to 0$, and the existence of this is not surprising given the fact that the dynamo can arise from the $\boldsymbol{B} \cdot \nabla \boldsymbol{b} + \boldsymbol{b} \cdot \nabla \boldsymbol{B}$ term in the induction equation. This term can be shown to be negative using the same integration by parts method used to obtain Eq. (C2), with the requirement $\omega\, dW/d\omega \leqslant 0$. The Pm dependent second term is obviously negative due to the positive definiteness of the integrand.

3. Pm ≫ 1

Inserting $\nu = \mathrm{Pm}\,\eta$ into Eq. (33), and carrying out a series expansion about $\mathrm{Pm} = \infty$ (see the previous section), one obtains

$$(\eta_{yx})_b^S \approx \frac{16\pi}{15} \int d\omega dk\, W_b k^2 \left(\frac{1}{\mathrm{Pm}} \frac{(\omega^2 - \tilde{\eta}^2)}{(\tilde{\eta}^2 + \omega^2)^2} + \ldots \right). \tag{C5}$$

As expected, there is no $\nu = 0$ contribution to the transport. Again using integration by parts, it is easy to prove negativity of the integral provided $\omega\, dW/d\omega \leqslant 0$.

[1] H. K. Moffatt, *Magnetic Field Generation in Electrically Conducting Fluids* (Cambridge University Press, Cambridge, England, 1978).
[2] F. Krause and K. H. Rädler, *Mean-field Magnetohydrodynamics and Dynamo Theory* (Pergamon, Oxford, 1980).
[3] J. F. Hawley, C. F. Gammie, and S. A. Balbus, Astrophys. J. **440**, 742 (1995).
[4] G. Lesur and G. I. Ogilvie, Astron. Astrophys. **488**, 451 (2008).
[5] R. M. Kulsrud and S. W. Anderson, Astrophys. J. **396**, 606 (1992).
[6] A. V. Gruzinov and P. H. Diamond, Phys. Rev. Lett. **72**, 1651 (1994).
[7] S. I. Vainshtein and L. L. Kichatinov, Geophys. Astrophys. Fluid Dyn. **24**, 273 (1983).
[8] A. Pouquet, U. Frisch, and J. Leorat, J. Fluid Mech. **77**, 321 (1976).
[9] I. Rogachevskii and N. Kleeorin, Phys. Rev. E **70**, 046310 (2004).
[10] K. H. Rädler, N. Kleeorin, and I. Rogachevskii, Geophys. Astrophys. Fluid Dyn. **97**, 249 (2003).
[11] V. V. Pipin, Geophys. Astrophys. Fluid Dyn. **102**, 21 (2008).
[12] J. Squire and A. Bhattacharjee, ApJ **813**, 52 (2015).
[13] J. Squire and A. Bhattacharjee, Phys. Rev. Lett. **115**, 175003 (2015).
[14] H. K. Moffatt and M. R. E. Proctor, Geophys. Astrophys. Fluid Dyn. **21**, 265 (1982).
[15] V. Urpin, Phys. Rev. E **65**, 026301 (2002).
[16] V. Urpin, Astron. Astrophys. **347**, L47 (1999).
[17] I. Rogachevskii and N. Kleeorin, Phys. Rev. E **68**, 036301 (2003).
[18] G. Rüdiger and L. L. Kitchatinov, Astron. Nachr. **327**, 298 (2006).
[19] K.-H. Rädler and R. Stepanov, Phys. Rev. E **73**, 056311 (2006).
[20] A. Brandenburg, K. H. Rädler, M. Rheinhardt, and P. J. Käpylä, Astrophys. J. **676**, 740 (2008).
[21] N. K. Singh and S. Sridhar, Phys. Rev. E **83**, 056309 (2011).
[22] G. Lesur and G. I. Ogilvie, Mon. Not. R. Astron. Soc. **391**, 1437 (2008).
[23] A. Brandenburg and D. Sokoloff, Geophys. Astrophys. Fluid Dyn. **96**, 319 (2002).
[24] A. Brandenburg, A. Nordlund, R. F. Stein, and U. Torkelsson, Astrophys. J. **446**, 741 (1995).
[25] O. Gressel, Mon. Not. R. Astron. Soc. **405**, 41 (2010).

[26] J. B. Simon, K. Beckwith, and P. J. Armitage, Mon. Not. R. Astron. Soc. **422**, 2685 (2012).
[27] E. G. Blackman and G. B. Field, Phys. Rev. Lett. **89**, 265007 (2002).
[28] N. Yokoi, Geophys. Astrophys. Fluid Dyn. **107**, 114 (2013).
[29] J. Squire, J. Burby, and H. Qin, Comput. Phys. Commun. **185**, 128 (2014).
[30] L. L. Kichatinov and G. Rüdiger, Astron. Astrophys. **260**, 494 (1992).
[31] G. Rüdiger and L. L. Kichatinov, Astron. Astrophys. **269**, 581 (1993).
[32] A. Yoshizawa and N. Yokoi, Astrophys. J. **407**, 540 (1993).
[33] A. Courvoisier, D. W. Hughes, and M. R. E. Proctor, Astron. Nachr. **331**, 667 (2010).
[34] T. Heinemann, J. C. McWilliams, and A. A. Schekochihin, Phys. Rev. Lett. **107**, 255004 (2011).
[35] D. Mitra and A. Brandenburg, Mon. Not. R. Astron. Soc. **420**, 2170 (2012).
[36] A. Brandenburg and K. Subramanian, Phys. Rep. **417**, 1 (2005).
[37] G. Rüdiger, Geophys. Astrophys. Fluid Dyn. **50**, 53 (1990).
[38] See Supplemental Material at http://link.aps.org/supplemental/10.1103/PhysRevE.92.053101 for a *Mathematica* notebook containing the full calculation detailed in this article.
[39] S. Sridhar and K. Subramanian, Phys. Rev. E **79**, 045305 (2009).
[40] G. Rüdiger and V. V. Pipin, Astron. Astrophys. **362**, 756 (2000).
[41] G. Bodo, F. Cattaneo, A. Mignone, and P. Rossi, Astrophys. J. **787**, L13 (2014).
[42] L. L. Kichatinov and V. V. Pipin, Astron. Astrophys. **274**, 647 (1993).
[43] D. Moss, A. Shukurov, and D. Sokoloff, Astron. Astrophys. **343**, 120 (1999).
[44] M. Rozyczka, N. Joung Turner, and P. Bodenheimer, Mon. Not. R. Astron. Soc. **276**, 1179 (1995).
[45] C. Donnelly, Ph.D. thesis, Cambridge University, 2013.
[46] O. Gressel and M. E. Pessah, Astrophys. J. **810**, 59 (2015).
[47] E. T. Vishniac and J. Cho, Astrophys. J. **550**, 752 (2001).
[48] K. Subramanian and A. Brandenburg, Phys. Rev. Lett. **93**, 205001 (2004).
[49] F. Ebrahimi and A. Bhattacharjee, Phys. Rev. Lett. **112**, 125003 (2014).
[50] E. N. Parker, Astrophys. J. **408**, 707 (1993).
[51] S. M. Tobias, Astrophys. J. **467**, 870 (1996).
[52] I. Rogachevskii, N. Kleeorin, and E. Liverts, Geophys. Astrophys. Fluid Dyn. **100**, 537 (2006).
[53] E. G. Blackman and J. C. Tan, Astrophys. Space Sci. **292**, 395 (2004).
[54] T. A. Yousef, T. Heinemann, A. A. Schekochihin, N. Kleeorin, I. Rogachevskii, A. B. Iskakov, S. C. Cowley, and J. C. McWilliams, Phys. Rev. Lett. **100**, 184501 (2008).